Charles University

Faculty of Mathematics and Physics

HABILITATION THESIS

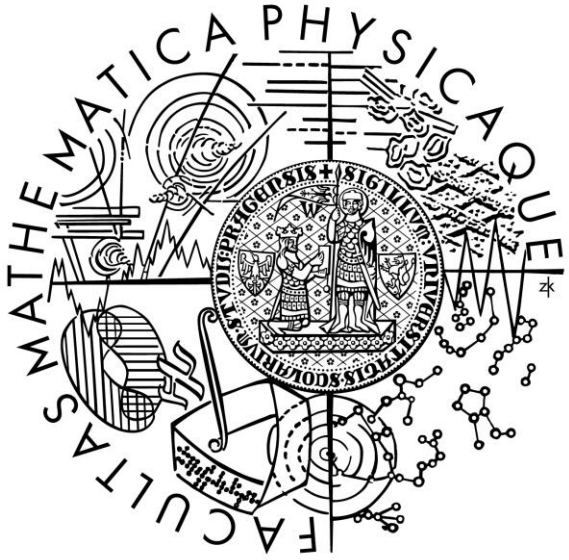

The role of single crystals in materials research

Jiří Pospíšil

Physics - Condensed Matter Physics

Prague 2021

Preface

This habilitation thesis consists of a set of 18 published scientific works I have authored or coauthored in the course of the last 10 years reprinted in the Appendix and a unifying commentary forming the thesis body. My studies of single crystals contributed to several fields of physics namely condensed matter physics and particularly in the field of magnetism of actinide systems. The underlying message of all the studies highlights the necessity and/or advantages of studies of bulk materials in the single crystal form, especially evident in the case of systems with highly anisotropic properties.

One part of the collected scientific results in this habilitation work was carried out in Prague at the Faculty of Mathematics and Physics of Charles University, in laboratories of the Department of Condensed Matter. The second part of the works was produced during my three years postdoc stay at Japan Atomic Energy Agency in the Advanced Science Research Centre in the group of Advanced Nuclear Materials Science in Tokai-mura, Japan.

Acknowledgments

I wish to express gratitude to colleagues and students from the Department of Condensed Matter Physics Prof. RNDr. Vladimír Sechovský DrSc., Doc. RNDr. Martin Diviš, CSc., Prof. Pavel Javorský, Dr., RNDr. Jan Prokleška, Ph.D., RNDr. Klára Uhlířová, Ross H. Colman and RNDr. Jana Šmilauerová Ph.D. for their friendship, support, trust, patience, excellent collaboration, and stimulating scientific discussions.

The great thank belongs also to my colleagues from Japan Atomic Energy Agency in Tokai, Japan, for their support during my 3 years postdoc stay in their group namely Yoshinori Haga, Shinsaku Kambe, Naoyuki Tateiwa, Yo Tokunaga, and Etsuji Yamamoto. I further thank all my co-workers from The Tohoku University branch in Oarai, namely Fuminori Honda, Ai Nakamura, and Dai Aoki, and co-workers Atsushi Miyake, Yoshimitsu Kohama, Jun Gouchi, Prof. Tokunaga, and Prof. Uwatoko from the Institute for Solid State Physics of the University of Tokyo.

I would like to stress out the significant contribution of my bachelor, diploma, Ph.D. students RNDr. Marie Hrůzová Kratochvílová, Ph.D. Mgr. Michal Vališka PhD., Mgr. Petr Opletal, Mgr. Kateřina Hanzlíková, Mgr. Petr Proschek, Bc. Anežka Bendová, Akinari Koriki, and Ing. Dávid Hovančík. Substantial parts of this work were supported by the Czech Science Foundation. The work was a part of the activity of the Charles University Research Centre (UNCE). The parts of the work have been also performed and supported by research infrastructures programs (ILL Grenoble). I acknowledge these supports.

In the end, I would like to thank my wife and family for their support in my work.

.....

RNDr. Jiří Pospíšil Ph.D.

Contents

1 Introduction

This work is a summary of the original works and results collected by the author with a primary focus on magnetism and electronic phenomena in 5*f* electron uranium intermetallic systems. The author has concentrated on the effect of external variables (temperature, magnetic field, doping, and pressure) on the stability and transitions among various magnetic states and paramagnetic regimes and the development of strongly correlated electron states in uranium systems. Because of the strong magnetocrystalline anisotropy of these systems, the growth of high-quality single crystals of the studied materials was the essential step to obtain the experimental results presented in this work.

The author significantly contributed to the development of single crystal growth methods and instruments in the home Department of Condensed Matter Physics within the MGML open access research infrastructure (see MGML.eu). The resulting rich single crystal growth instrumentation in the home institution has enabled the preparation of other classes of materials. Their summary and author's contribution are commented on in Chapter 6.

1.1 The concept of magnetism in uranium intermetallic systems

Since the majority of 4*f* electron density in lanthanides is deeply embedded within the core of an ion, the interaction of the 4*f* states with the environment is very weak and the magnetic exchange interaction is provided by the polarization of the conducting electrons-so called RKKY interaction. Consistently, the observed ground state magnetic moments of regular lanthanide ions usually well agree with the corresponding RE^{3+} free-ion values ($g_J\mu_B J$) calculated within the *LS* coupling scheme. Contrary, the 5*f* wave functions in actinides are more extended in space, and thus exposed to a much stronger interaction with the metallic environment, compared to the 4*f* case. Consequently, the 5*f* electrons in actinides are, as a rule, delocalized due to their participation in bonding, and hence a considerable hybridization of the 5*f* states with the valence states of neighboring atoms (5*f*-ligand hybridization) exists in the crystal lattice. This applies particularly for light actinides up to Pu.

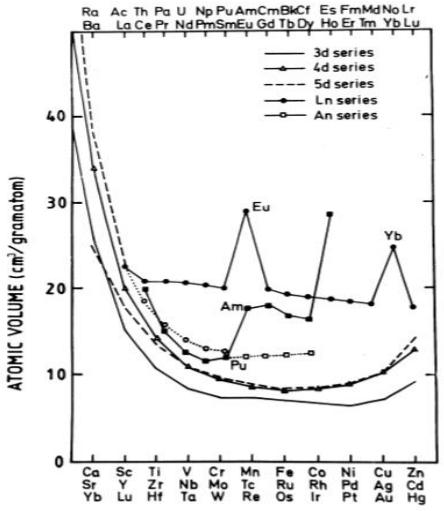

Figure 1.1 Evolution of atomic volume across 3*d*, 4*d*, 5*d*, 4*f*, and 5*f* transition metals series. The picture was taken from Ref.[1]

The itineracy of the actinides 5*f* electrons develops throughout the period. According to Johansson and Skriver's model, the contribution to bonding by light

actinides is more significant than that in the heavy actinides Figure 1.1 reflected in the step of atomic volume.

Hence the light actinides up to plutonium resemble the band-like behavior of transition metals. However, between plutonium and americium, there is a dramatic change and the volume increases by about 50%. The heavy actinides atomic volumes, from the americium, behave very similar to the lanthanides. The Pu and Am compounds are the best candidates from the point of view of investigation of strongly correlated electronic phenomena; however, the studies are very limited due to their high radiation. Irrespective of difficulties, the Pu superconductors with the highest superconducting transitions among the so far explored actinides-$PuCoGa_5$ and $PuCoIn_5$ were reported[2-4].

From this point of view, U intermetallics are still located in the vicinity of the boundary between localized and itinerant characters. The magnetism of the uranium compounds is mostly affected by 5*f*-5*f* direct overlap of the wave functions of the nearest ion neighbors ($d_{U\text{-}U}$). Therefore, a shorter distance between uranium atoms leads to a larger overlap of the 5*f* functions, which causes the breaking of the Stoner criterion[5] and the magnetic order does not occur. It indicates the importance of the distance parameter between uranium atoms related to the magnetic features, which was first realized by H.H. Hill[6]. He derived a certain critical distance between Uranium atoms called Hill's limit, separating non-magnetic (superconducting) ground state compounds and magnetic ground state compounds. The value of the critical distance was empirically established in the range of $d_{U\text{-}U}$ = 3.4 - 3.6 Å. Most materials follow this behavior (Figure 1.2).

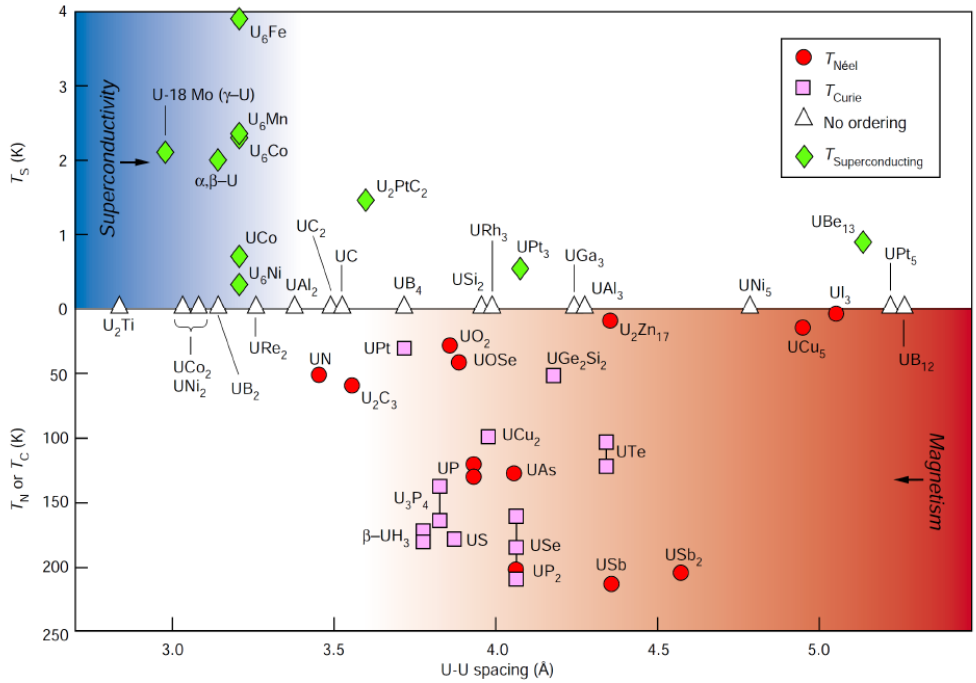

Figure 1.2 The Hill's plot[7], modified by W. Knafo[8].

Generally, two one-electron mechanisms can be considered as affecting the character of the 5*f* states. The first one is the already described 5*f* electron hopping due to the overlap of the 5*f* wave functions from neighboring U-sites leading to the formation of the narrow 5*f* band. The second mechanism, hybridization with wave functions of the surrounding ions, has a dual role. In the first approximation, it is a primary mechanism of the destabilization of 5*f* moments, in the second approximation, because the spin information can be conserved in the course of the hybridization process, it mediates indirect exchange coupling. The maximum ordering temperatures can be consequently expected for a moderate strength of hybridization, because a strong hybridization

completely suppresses magnetic moments, whereas a weak one leaves moments intact, but their coupling is weak[9].

The exchange interactions between the existing 5*f* moments in actinide intermetallics considerably involve the corresponding 5*f* wave functions. Hence it is typically much stronger than for the 4*f* moments interacting only via the RKKY interaction. The impact of delocalization on magnetic excitations is even more dramatic. No crystal field excitations could be observed by inelastic neutron scattering in the vast majority of uranium intermetallics studied so far. Instead, one observes typically a rather broad quasielastic response reflecting the 5*f*-moment instability in analogy to, e.g., cerium mixed-valence materials. The delocalized 5*f* states in U intermetallics give rise to an essentially different mechanism of magnetic anisotropy based on two-ion (5*f*-5*f*) interactions.

1.2 The issue of magnetic phases, transitions, and crossovers

The phase transition defines the moment when the system changes its thermodynamic properties as a response to variation of the external conditions, most often temperature. The phase transitions are traditionally classified into first-order and continuous second-order types. At first-order transitions, the two phases co-exist at the transition temperature, a typical example is the melting of the ice. On the other hand, at continuous second-order transition, the two phases do not co-exist. An important example of the second-order transition is the ferromagnetic (FM) or superconducting (SC) transition. The transition point during the continuous phase transition is also called the critical point.

The phase transitions mentioned above occur at a finite temperature and macroscopic order is destroyed by thermal fluctuations. However, the phase transitions can be initialized not only as of the effect of temperature but upon variation of other types of external control parameters like pressure, magnetic field, or chemical doping. These non-thermally driven phase transitions have attracted the attention of physicists because the order of transition can vary and push the system to strange electronic states. Then, for example, low temperature magnetic field-induced metamagnetic spin-flip transition in highly anisotropic antiferromagnet (AFM) is a first-order type, which is projected to the phase diagram by the presence of a so-called tricritical point (TCP). At TCP the first-order transition transforms to the standard second-order magnetic transition. Surprisingly, the recent intensive studies of strongly anisotropic FMs have revealed, that the original second-order transition can also systematically transform to field-induced first-order transition at TCP, as well[10-12].

The special class of transitions are those taking place at zero temperature where quantum fluctuations extend the systems about other dynamic dimensions, which strongly depends on the dimensionality of the system and the degree of freedom. The variation of the non-thermal control parameters can lead the systems to the so-called quantum critical point (QCP) and quantum phase transition (QPT)[13]. Experimental development and theoretical progress in the last decades have made clear that the presence of QPT plays an important role in the unsolved puzzles in heavy-fermion compounds[14]. The physical properties of the quantum fluctuations, which can destroy long-range order at absolute zero temperature, are quite distinct from those of the thermal fluctuations responsible for traditional, finite-temperature phase transitions[13, 15, 16]. At the quantum critical point, the low-temperature thermodynamics is characterized by collective modes corresponding to fluctuations of the order parameter, rather than by single-fermion excitations as in a Fermi liquid. Therefore, non-Fermi-liquid properties arise. The temperature dependencies strongly depend on the dimensionality *d* of the system and the nature of the interactions[17].

A lot of efforts have been invested in this issue particularly in actinide systems or 4*f* electron systems with valence instability (Ce and Yb). The intensive research has revealed that besides ordinary magnetic phases like FMs or antiferromagnets (AFMs), series of strongly correlated electron phases and regimes can arise under the application of external non-thermal as well as the character of the phase transition can develop[18].

1.3 Magnetic phase diagrams of uranium intermetallic

From the point of view of systematic exploration of so far unknown electronic states and phenomena, uranium intermetallics with the nearest U ions distance respecting the Hill's limit are the promising candidates. Particularly the application of hydrostatic pressure is the effective parameter. The pressure, typically in the range of tens of GPa, is sufficient capable to bring the nearest U ions closer together, which makes the 5*f* band broader, reducing the density of 5*f* states at Fermi level and thus suppressing magnetism.

Unfortunately, the preparation of pressure experiments is expensive and time-consuming. An alternative approach is via doping of the systems by suitable ions with a larger or smaller diameter than the original one, which leads to shrinking or expansion of the crystal lattice. This method allows quite a simple exploration of the phase diagrams, however, the results are often affected by the induced disorder in the lattice as well as by the distribution of the dopant and its participation in the band structure, all effects and their contributions are hardly predictable.

The magnetism of uranium compounds is quite well theoretically predictable by ab initio calculation on the electron level, where the effects of 5*f* wave function overlap, hybridization, and electron transfers are treated. On the other hand, many-body interactions, which give rise to emergent phenomena, are behind the framework of one-electron theories. Due to the character of the 5*f* wave functions, even tiny external effects can have a strong impact on the resulting electronic state in such a situation. Therefore, detailed experimental studies focused on the search for new materials and construction of their two or even three-dimensional phase diagrams are indispensable to unveil the physics of uranium 5*f* electron systems.

Knowledge of the global landscape of U compounds gave marked success in the discovery of many uranium compounds with electronic properties, which often do not have any parallel in other solid-state systems. The coexistence of AFM and SC was discovered in UPd_2Al_3[19, 20] compounds, heavy-fermion SC in UBe_{13}[21] or UPt_3[22-25] with complex SC phases, respectively. The unique case is the hidden ordered state coexisting with unconventional SC in URu_2Si_2, the microscopic mechanism of which remains an unresolved issue irrespective of experimental and theoretical efforts for the last decades[26-29].

The remarkable uranium compounds in the fore of nowadays interest of the solid-state physics community are ferromagnetic superconductors (FM SCs). This group consists of only three members UGe_2[30], URhGe[31], and UCoGe[32]. While the area of superconductivity (SC) is pressure-induced in UGe_2 on the boundary of two FM phases, the mutual coexistence of ferromagnetism (FM) and SC in URhGe and UCoGe appear at ambient pressure.

All three compounds join orthorhombic structures (UCoGe and URhGe are isostructural crystallizing in TiNiSi-type structure) where U ions are arranged to the characteristic zig-zag chain with the $d_{(U\text{-}U)}$ parameters close to Hill's limit. Therefore, the magnetism, particularly in the case of UCoGe, is naturally very unstable, as reflected by very low Curie temperature T_C = 2.5 K and spontaneous moment only μ_{spont} = 0.07 μ_B/f.u. At such systems, critical spin fluctuations (SFs) can give ri to an unconventional SC state. Within further intensive research of similar orthorhombic compounds, a heavy-fermion

SC has been discovered very recently in UTe_2[33, 34]. It also crystallizes in orthorhombic crystal structure with a similar zig-zag arrangement of U ions. The critical $d_{(U-U)}$ distance is just below Hill's limit and no sign of ordinary magnetic order was detected down to the lowest temperatures. However, very strong SFs are still present in this material and SC state appears at a significantly higher critical temperature (T_{SC} = 1.6 K) than that of in FM SCs.

The characteristic feature of these systems in the vicinity of magnetic instability is very high sensitivity on external parameters like a magnetic field, temperature, doping, or external pressure. Its application strongly affects, usually suppresses, the unstable magnetic ground states with simultaneously enhanced critical spin fluctuations. It is projected in exotic phase diagrams with a rich variety of phases and correlated electronic states separated by ordinary type of phase transitions or various crossovers[35-37].

The complexity of the real magnetic phase diagram of 5*f* electron systems can be well demonstrated by angular-dependent *H-T* or *p-T* phase diagrams of FM SCs and UTe_2, respectively. The re-entrant superconductivity was detected in FM SCs or multiple superconducting phases were detected under pressure in UTe_2[38] as well as the exotic field-induced superconducting state was re-enforced above critical magnetic field H_{c2} when the sample was oriented 27±5° from the crystallographic direction *b* towards *c*[39].

1.4 Motivation and structure of the work

The motivation of the work is the analysis of the complex magnetic phase diagrams of uranium 5*f* electron systems naturally located near the Hill's limit concerning the development of the character of the phase transitions, crossovers connected with various types of paramagnetic regimes, and the rise of strongly correlated electron phenomena as a function as external variables-temperature, magnetic field, chemical doping, and pressure.

The work combines two working branches. The synthesis of the well-known but not properly studied uranium materials or completely new materials in the form of high-quality single crystals thanks to unique equipment of the home laboratories in DCMP and ASRC, JAEA Tokai, Japan where I was staying as a postdoc for three years position. In the second step, all materials were studied as a function of the above listed external parameters using in-house instrumentation as well as in frequent cooperation with other scientific institutions, namely Institut Laue-Langevin in Grenoble, The University of Tokyo, and Tohoku University in Japan.

The work is organized into 8 chapters. Chapter 1 is dedicated to an introduction to the subject; Chapter 2 summarizes the contribution to the physics of uranium FM SCs and related isostructural compounds; Chapter 3 – summary of results in UTX compounds of hexagonal ZrNiAl-structure type, Chapter 4 – summary of results on newly discovered U_2Rh_2Pb compound; Chapter 5 – general trends of magnetism in ordered uranium systems and Chapter 6 – summary of author's contribution to various systems in cooperation with the colleagues and scientific partners in the sense of growth of single crystals of new materials. The last Chapter 7 summarizes the conclusions of the author's work.

2 Magnetism of orthorhombic UTX compounds

The ternary orthorhombic compounds of UTX composition (T – transition metal, X – *p*-element) represent a broad group of uranium materials that are at the fore of

scientific interest in the field of heavy-fermion physics and unconventional superconductivity, particularly FM SCs UCoGe and URhGe. The general structure is displayed in Figure 2.1.

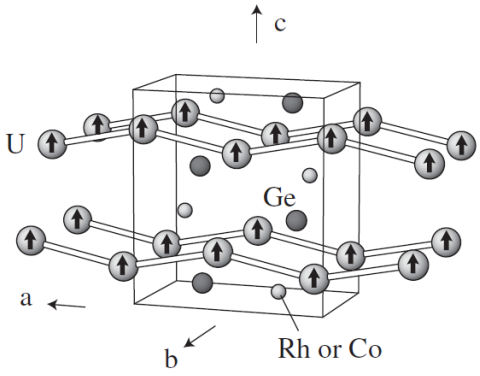

Figure 2.1 The arrangement of the ions in the orthorhombic TiNiSi-type structure. The uranium ions create a zig-zag chain along the *a*-axis along which the nearest uranium neighbor distance $d_{U\text{-}U}$ is present[40].

UCoGe is FM with T_C = 2.5 K and SC appears at T_{SC} = 0.6 K[32] (both parameters strongly sample dependent[41, 42]), URhGe orders at T_C = 9.5 K and SC appears at T_{SC} = 0.25 K[31].

We have arranged the all known orthorhombic UTGe compounds according to Hill's scenario[7] (Figure 2.2) and realized that URuGe with smaller $d_{U\text{-}U}$ < 3.45 Å is paramagnets, two FMs UCoGe a URhGe are present in the vicinity of Hill's limit $d_{U\text{-}U}$ = 3.5 Å and all compounds with $d_{U\text{-}U}$ > 3.5 Å are AFMs, all magnetic compounds with gradually increasing ordering temperature.

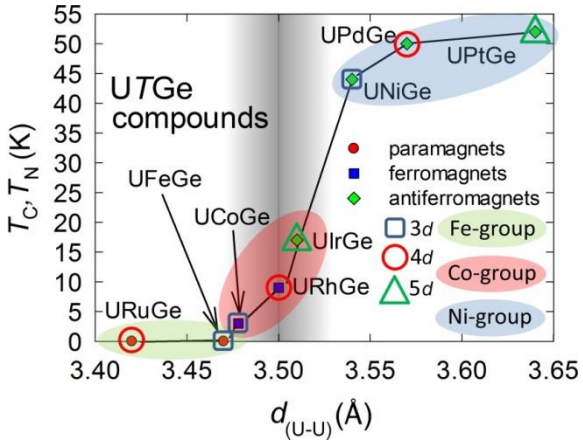

Figure 2.2 Illustrative Hill's plot showing the dependence of the ordering temperature of the UTGe compounds as a function of the shortest distance between two nearest uranium atoms($d_{U\text{-}U}$). The shaded region spreads around Hill's limit (3.5 Å). The position of UFeGe is exceptional because UFeGe, as well as UPtGe, do not order in the TiNiSi-type structure[43-46].

It has been observed that the Ru or Fe substitution rapidly stabilizes the FM state[47] in UCoGe, even though URuGe and UFeGe behave like Pauli paramagnets down to the lowest temperatures[48-50]. A similar increase of T_C was reported in the case of the initial substitution of Co and Ru for Rh in URhGe[51, 52] with the development of a non-Fermi-liquid (NFL) state on the higher doping boundary of the FM dome[51]. Within this chapter,

we have studied the effect of alloying on the stability of the magnetic state of UCoGe - $UCo_{1-x}Ru_xGe$, $UCo_{1-x}Rh_xGe$, and $UCo_{1-x}Ir_xGe$, supported by microscopic studies of magnetism by polarized neutron diffraction (PND). In the second step, the interest was focused on AFM counterpart UIrGe, which is still located in the vicinity of Hill's limit but from the opposite side than UCoGe. Series of high magnetic field and high-pressure experiments have been performed to reveal the aspects of magnetism of this interesting compound.

2.1 Study of alloying variants of FM SCs UCoGe and URhGe

2.1.1 Magnetism and phase diagram of $UCo_{1-x}Ru_xGe$ system [P1]

Substitution of UCoGe by Ru was our initial work. To study the development of the magnetic and SC state throughout the $UCo_{1-x}Ru_xGe$ system we prepared a series of polycrystalline samples with different Ru concentrations x between 0 and 0.9. We have investigated the samples by x-ray diffraction, magnetization, specific heat, and electrical resistivity measurements.

We have detected that the initial Ru substitution up to $x = 0.1$ leads to a stabilization of the weak FM state of UCoGe projected as the simultaneous sharp increase of the Curie temperature and spontaneous magnetization up to maximum values of $T_C = 8.6$ K and $M_S = 0.1\mu_B$/f.u. respectively, whereas superconductivity vanishes already for $x = 0.03$. Further increase of the Ru content beyond $x = 0.1$ leads to a precipitous decrease of both T_C and M_S towards a FM QCP at $x_{cr} = 0.31$. Consequently, the $T - x$ magnetic phase diagram (Figure 2.3) consists of a well-developed ferromagnetic dome. Further evidence for the FM QCP is offered by the rapid increase of the effective mass of the quasiparticles near x_{cr}. The proposed scenario is also corroborated by scaling of the ordering temperature with the control parameter itself which obeys the formula $T_C \sim (x_{cr} - x)^{3/4}$ and provides an estimate of the critical concentration $x_{cr} = 0.31$. The FM transition of $UCo_{1-x}Ru_xGe$ compounds in the vicinity of x_{cr} is apparently of a second-order type in contrast to the first-order transition reported for three-dimensional FMs in the vicinity of a QCP[11, 53]. The analysis of the temperature dependencies of the electrical resistivity and specific heat at low temperatures of the samples in the vicinity of the QCP reveals a non-Fermi-liquid behavior and assigns the FM QPT to be most likely of a continuous Hertz-Millis type[17, 54, 55].

Considering the change of the $d_{U\text{-}U}$ between the nearest U neighbor ions within the $UCo_{1-x}Ru_xGe$ series, we find that $d_{U\text{-}U}$ decreases with increasing Ru concentration from ≈ 3.48 Å in UCoGe to 3.44 Å in URuGe. Both values fall rather into the "nonmagnetic side" of the Hill plot[7]. On the other hand, one should bear in mind that each U ion has only two nearest U neighbors on the $d_{U\text{-}U}$ chain meandering along the a-axis. If the 5f -5f overlap was the only mechanism controlling magnetism, then a gradual washout of U magnetic moment and monotonous decreasing of T_C with increasing Ru content would be expected. However, we have observed an initial rapid increase of T_C. We note that our observation of the FM dome in the magnetic phase diagram in $UCo_{1-x}Ru_xGe$ is similar to those observed for $UCo_{1-x}Fe_xGe$[56], $URh_{1-x}Ru_xGe$[51], and $URh_{1-x}Co_xGe$[52].

An additional mechanism, namely, the 5f -ligand hybridization, must be taken into account for conceiving the complex evolution of FM in these systems. One solution based on theoretical band structure calculation provides the mechanism responsible for the FM dome in the magnetic phase diagram of $UCo_{1-x}Ru_xGe$ by following the simple model treating the changes of 5f - nd hybridization with variations of the widths and mutual positions on the energy scale of the transition metal d bands and U f bands[57]. Accordingly, the non-isoelectronic substitution of Co by Ru causes broadening of the d

band from 3*d* to 4*d* transition-metal-like. Together with the mutual movement of the *d* and *f* bands on the energy scale itself, we could qualitatively conceive the dome-like dependence of the T_C.

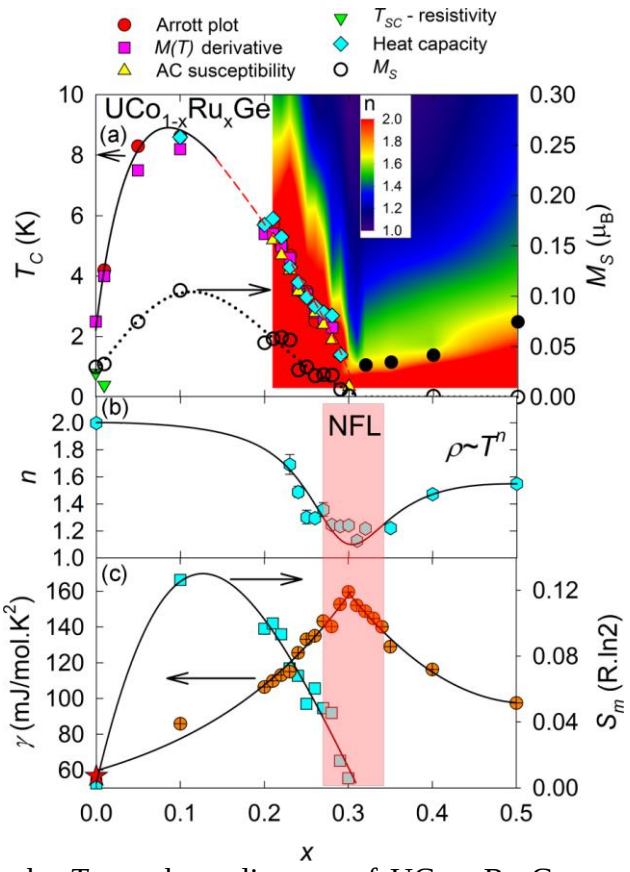

Figure 2.3 Panel (a) the $T - x$ phase diagram of $UCo_{1-x}Ru_xGe$ system. The diagram is supplemented by the results of the electrical resistivity measurement revealing the occurrence of SC in the parent UCoGe compound and in $UCo_{0.99}Ru_{0.01}Ge$ the two data points are taken from Ref.[47](green triangle). The black solid line is only a guide to the eye, while the red dashed part is a fit of $T_C \sim (x_{cr} - x)^{3/4}$. The right axis denotes the spontaneous magnetization M_S (the dashed line in the plot is only a guide to the eye). The color plot shows local exponents of the resistivity obtained as $n = d \ln(\rho - \rho_0)/d \ln T$. The black-filled circles show the temperature where resistivity starts to deviate from the T^2 dependence. Panel (b) shows the evolution of the coefficients n from the fitting of the low-temperature dependence of the electrical resistivity with equation $\rho = \rho_0 + AT^n$ for $T > T_C$. The right vertical axis shows RRR = $\rho_{300\,K}/\rho_{0.4\,K}$ as a function of x. Panel (c) shows the development of C/T (extrapolated to 0 K) and the magnetic entropy S_m (value for UCoGe is taken from Ref.[58].

2.1.2 PND study of ferromagnetism of UCoGe [P2]

The result of the previous study of $UCo_{1-x}Ru_xGe$ system with the increase of T_C and the dome of stable FM phase motivated us to perform a microscopic magnetic study to reveal the origin of such behavior. The FM state of UCoGe was considered rather complex as Co exhibits a large magnetic moment and thus significantly contributes to the total ordered magnetic moment. The polarized neutron diffraction (PND) experiments on UCoGe at 0.1 K and magnetic field of 12 T showed an induced moment on the Co site that compares to the uranium moment and is antiparallel to it[59]. Macroscopic measurements were also consistent with a transition to a ferrimagnetic state in high

magnetic fields[60]. However, the reported polarization of the Co magnetic moment antiparallel to the U magnetic moment contrasts with the behavior found in another FM UTX (X = Al, Ga, Si, and Ge) compounds, for which the U and T moments are always found to be parallel, e.g. URhSi[61], UCoAl[62, 63], URhAl[64], URuAl[65].

For our experiments, we have prepared two substituted UCoGe single crystals with compositions $UCo_{0.97}Ru_{0.03}Ge$ (still in the vicinity of UCoGe) and $UCo_{0.88}Ru_{0.12}Ge$ (the highest T_C) and studied them by PND. The PND experiment on $UCo_{0.88}Ru_{0.12}Ge$ was carried out at the D3 diffractometer in ILL 1.65 K, well below the ordering temperature. For $UCo_{0.97}Ru_{0.03}Ge$, the experiment was carried out at the 5c1 diffractometer of LLB in Saclay. Spin densities were deduced from the obtained magnetic structure factors through a maximum entropy reconstruction[66-68]. The results (i.e. magnetization density maps with the highest probability) are shown in Figure 2.4.

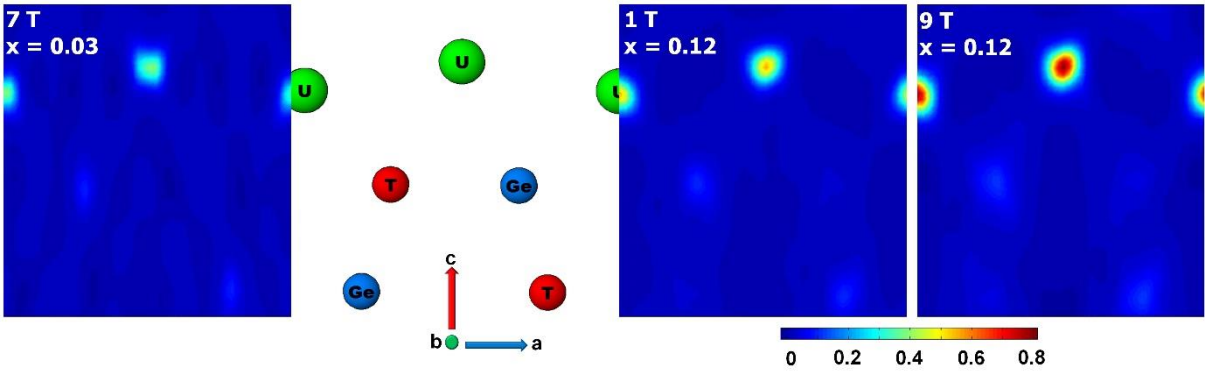

Figure 2.4 Magnetization densities in the (x, y = 0.25, z) plane for $UCo_{0.88}Ru_{0.12}Ge$ in applied magnetic fields of 1 T and 9 T || c and $UCo_{0.97}Ru_{0.03}Ge$ in the applied magnetic field of 7 T || c. The scale of all maps is $m\mu_B$/cell. T labels the mixed Co/Ru site.

The Co magnetic moments are oriented parallel to the U moments in both compounds, contrary to what is observed in the parent compound UCoGe[59]. Moreover, our result was in agreement with parallelly running synchrotron radiation studies (X-ray magnetic circular dichrorism[69, 70] and Compton scattering[71]). We concluded that the magnetic state of UCoGe is not anomalous and a common ferromagnetic state was found, with the U and Co magnetic moments parallel to each other.

We have also integrated the magnetization densities in a defined volume to estimate the absolute value of the magnetic moments centered on the U and Co ions. For this purpose, we choose simple spheres centered on atomic positions. The results are summarized in Table III in the original manuscript[72]. In the dipole approximation, the magnetic form factor on the uranium site was decomposed into orbital μ_L^U and spin μ_S^U contributions. The orbital part μ_L^U is the leading part in both compounds and is parallel to the applied magnetic field. The weaker spin part, μ_S^U, is coupled antiparallel to μ_L^U, similar to what has been observed in many uranium-based compounds[61, 62] including UCoGe[59, 71].

The $|\mu_L^U/\mu_S^U|$ ratio carries indirect information about the hybridization strength within the selected systems[73]. The smaller $|\mu_L/\mu_S|$ ratio reflects the strong hybridization with the *s*, *p*, *d* valence states and the direct overlap of the 5*f* wave functions (intermediate coupling). Generally, a high value of $|\mu_L^U/\mu_S^U|$ reveals a higher localization of the 5*f* electrons: the μ_L^U density in U intermetallics is usually distributed closer to the ion center than the spin density[74, 75]. We have plotted the $|\mu_L^U/\mu_S^U|$ ratios as a function of T_C (Figure 2.5). There is a clear increase of the $|\mu_L^U/\mu_S^U|$ ratios from $UCo_{1-x}Ru_xGe$ towards URhSi. Thus, the hybridization strength as delocalization mechanism is the lowest in ferromagnetic URhSi where the 5*f* states are much localized within the TiNiSi-

type UTX family[76]. The $|\mu_L^U/\mu_S^U|$ ratios for Ru substituted UCoGe single crystals lie between the expected UCoGe and URhSi ones, signaling that the 5*f* states are more localized than in the parent compound UCoGe and that the hybridization strength as delocalization mechanism is weaker. However, the low absolute values of μ_L^U and μ_S^U indicate that $UCo_{0.97}Ru_{0.03}Ge$ and $UCo_{0.88}Ru_{0.12}Ge$ and even URhSi can be still classified as itinerant ferromagnets. Moreover, the gradual localization of the 5*f* states in $UCo_{0.97}Ru_{0.03}Ge$ and $UCo_{0.88}Ru_{0.12}Ge$ deduced from $|\mu_L^U/\mu_S^U|$ ratios is in very good agreement with the relevant physical quantities obtained from our macroscopic measurements. We have found systematic scaling of the specific heat jumps $\Delta C_p/T$ proportional to magnetic entropy at T_C for TiNiSi-type UTX compounds – see Figure 2.5.

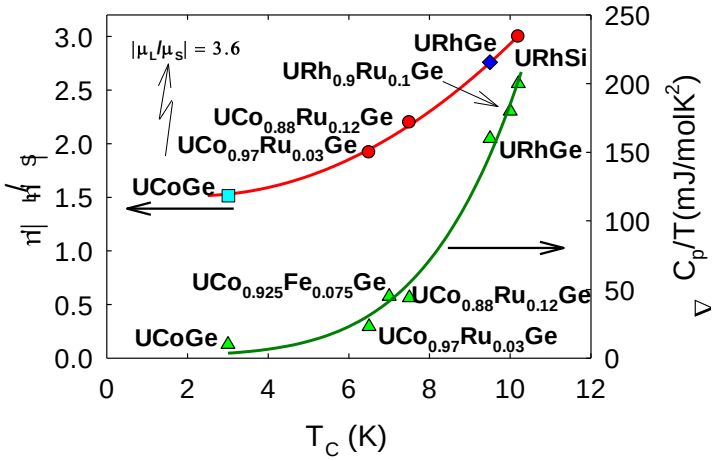

Figure 2.5 Evolution of the $|\mu_L^U/\mu_S^U|$ ratio and of the magnitude of specific heat jumps $\Delta C_p/T$ with T_C in the TiNiSi-type ferromagnetic UTX compounds. The blue point suggests the expected value of the $|\mu_L^U/\mu_S^U|$ ratio in URhGe where experimental data are still missing. The cyan point suggests the expected value of the $|\mu_L^U/\mu_S^U|$ ratio for the UCoGe respecting $\Delta C_p/T$ scaling. The URhSi value of $|\mu_L^U/\mu_S^U|$ was taken from data available in Refs.[61], $\Delta C_p/T$ are taken from Refs.[32, 56, 76]. The solid lines are guides to the eye.

Our PND study confirmed that the initial growth of T_C and $\mu_{spont.}$ ($x \leq 0.12$) in $UCo_{1-x}Ru_xGe$ is due to the weakening of hybridization strength as a delocalization mechanism. Based on our study, we have concluded the standard arrangement of components of magnetic moments in UCoGe. The most localized 5*f* electrons within the series are in URhSi and URhGe, even so, the localization of the 5*f* states is still far from typical local moment ferromagnets like UAsSe[77].

2.1.3 Magnetism in $UCo_{1-x}Rh_xGe$ system [P3]

The 5*f*-electron FMs URhGe[31] and UCoGe[32] exhibit strong magneto-crystalline anisotropy. The metamagnetic-like phenomena occur in UCoGe and URhGe when a magnetic field is applied along the orthorhombic *b*-axis resulting in the famous magnetic-field-induced reentrance of SC in their *H*-*T* phase diagrams[78-80]. A jump in the magnetization of URhGe for $H \parallel b$ is observed at a characteristic field of ≈ 12.5 T (in the literature marked as H_R[81, 82]). This anomaly reflects a first-order metamagnetic phase transition (FOMPT) to polarized paramagnetic state (PPM) involving the reorientation of the magnetic moment from the *c* to the *b*-axis[83, 84] leading to a loss of ferromagnetic ordering. This process induces strong FM spin fluctuations and the field-induced

reentrant SC phase has the sharp maximum in the vicinity of H_R and vanishes just above the H_R[79].

On the other hand, the *b*-axis magnetization of UCoGe at 1.5 K shows an upturn in the magnetization isotherm at ≈ 47.5 T[78] (in the literature marked as H_m[78]) which is more than three times higher on an energy scale than the field of ~15 T where the SC in UCoGe becomes reinforced[78, 85]. Moreover, in contrast to URhGe, the SC is suppressed by a magnetic field applied along *b* very little creating a broad, so far experimentally unbounded, superconducting dome with upper critical field H^b_{c2} exceeding 20 T[86, 87]. The field of the broad metamagnetic-like anomaly on the low-temperature magnetization isotherm in UCoGe is comparable in energy scale to a broad maximum in the temperature dependence of magnetic susceptibility, appears[18]. Such a maximum with the upper point at so-called T_{max}[18] was observed on the $\chi_b(T)$ curve for $H \parallel b$ axis of UCoGe at 37.5 K[78] which is far above T_C = 2.5 K. On the other hand, a sharp peak at $T_{max} = T_C$ = 9.5 K[78, 88, 89] was found for URhGe.

The remarkably different behavior of both FM SCs UCoGe and URhGe stimulated us to study the evolution of the characteristic magnetization behavior over the entire pseudoternary $UCo_{1-x}Rh_xGe$ system. SC in URhGe[83, 89] and UCoGe[87, 90, 91] have been intensively studied. In contrast, much less attention has been paid to the magnetization behavior in the normal state, particularly to the paramagnetic range in the neighborhood of the FM domes in their complex magnetic *H-T* phase diagrams.

For the research, we have prepared series of substituted $UCo_{1-x}Rh_xGe$ compounds with compositions x = 0.1, 0.2, 0.3, 0.4, and 0.8 in the form of single crystals by the Czochralski method in a tetra-arc furnace and investigated them primarily by magnetization in pulsed magnetic fields up to 57 T installed at the International Mega Gauss Science Laboratory of the Institute for Solid State Physics at the University of Tokyo - see results in Figure 2.6.

As illustrated by dashed lines in Figure 2.6, the metamagnetic-like anomalies were detected for all compositions at critical fields, which corresponds to identical values of magnetization (M_{ins} = 0.35 μ_B/f.u., $M_{inf.}$ = 0.41 μ_B/f.u. and M_{end} = 0.52 μ_B/f.u.). The initial slope of magnetization (dM/dH) at M_{ins} (see inset of Figure 2.6), is ~ five times larger (~31 mμ_B/T) for URhGe than for UCoGe (~7 mμ_B/T). We also note that this feature is conserved in the isostructural ferromagnet URhSi at the *b*-axis moment polarization crossover[92] and the *b*-axis metamagnetic transition (MT) of isoelectronic antiferromagnet UIrGe[93].

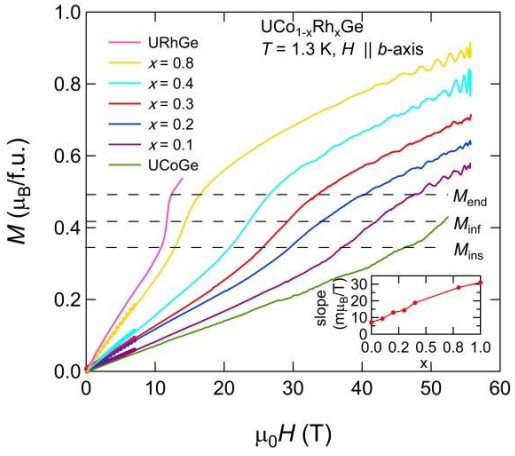

Figure 2.6 Magnetization isotherms of all $UCo_{1-x}Rh_xGe$ compounds measured in pulsed-field along the *b*-axis; data for parent compounds are identical to those reported in Ref. [78]

and displayed with kind permission of authors W. Knafo and D. Aoki. The inset shows the development of the magnetization slopes dM/dH at M_{ins}. The dashed lines indicate the onset M_{ins}, inflection M_{inf}, and the end M_{end} of the metamagnetic-like anomalies.

We have collected magnetic parameters from all the studied compounds and constructed the *T-x* and *H-x* phase diagrams of the $UCo_{1-x}Rh_xGe$ in Figure 2.7.

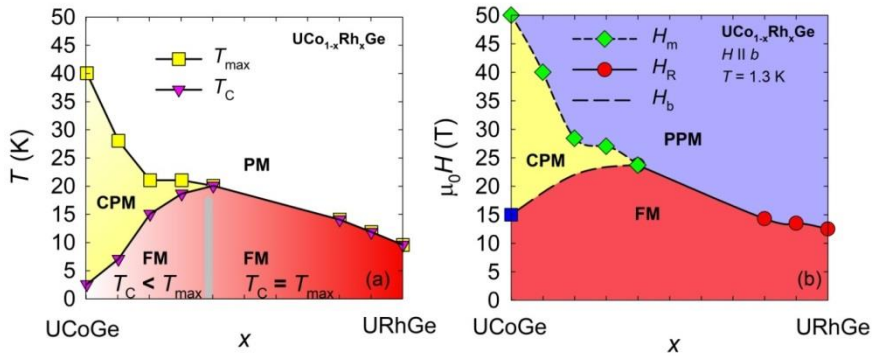

Figure 2.7 a) *T-x* and b) *H-x* phase diagrams of the $UCo_{1-x}Rh_xGe$ system. The value of T_{max}, $H_{R,}$ and H_m for URhGe and UCoGe, respectively, were taken from Ref. [78]. The blue point in panel (b) marks the critical field of the ferromagnetic phase boundary in UCoGe; the point was taken from Ref. [86]. The long-dashed line in the *H-x* diagram tentatively indicates the evolution of FM → CPM crossover at H_b. The grey line in the *T-x* diagrams in panel (a) tentatively separates the low- and high-S_{mag} concentration regions.

The *T-x* diagram of the $UCo_{1-x}Rh_xGe$ system has two distinctly different parts. For $x < 0.4$ the, *M(T)* dependences are characterized by the broad maximum in magnetic susceptibility at T_{max} showing up well above T_C while a sharp peak appears at $T_C = T_{max}$ on the URhGe side ($x \geq 0.4$). The region extends to the FM limit of the isoelectronic $URh_{1-x}Ir_xGe$ system[94], indicating that this phenomenon is very robust.

The maximum in magnetic susceptibility along the *b* is attributed to a crossover to the so-called correlated paramagnetic (CPM) regime[18, 37]. Thus, the cooling of the compounds with $0 < x < 0.4$ consists of PM-CPM crossover followed by a CPM-FM phase transition at T_C. In contrast, cooling of the compounds with $0.4 \leq x < 1$, results in a direct PM-FM phase transition at T_C. The detected metamagnetic fields H_m vary with *x* in quite the same manner as the value T_{max} with the proposed energy scale1 T ~ 1 K [18] in agreement with observations in recent examples[35, 93-96].

Our detailed knowledge of the transitions and crossovers between PM, CPM, PPM, and FM allows us to explain the different shapes of the superconducting re-entrant domes for both parent compounds. The FM $\xrightarrow{H_R}$ PPM FOMPT of Lifshitz type in URhGe is connected with an increase of both the longitudinal and transversal magnetic fluctuations supporting the SC state[89]. However, this FOMPT to the PPM resulting in a polarization of the magnetic moments towards the *b*-axis must necessarily lead to sudden freezing of the magnetic fluctuations. Therefore, the re-entrant SC sharply disappears above H_R. In contrast, the FM $\xrightarrow{H_b}$ CPM crossover in UCoGe does not polarize the magnetic moments. Therefore, it is not prohibitive for the spin fluctuations and the SC state can survive in the CPM to very high magnetic fields with the enormous value of $H_{c2(0)}$ [87] (and above p_c [97], where the CPM should exist, as well). The field-induced transition from the FM state in UCoGe and URhGe is different and terminates in different paramagnetic states, CPM and PPM, respectively.

2.2 UIrGe - Antiferromagnetism and its stability under external conditions

Isostructural FM SCs URhGe and UCoGe of TiNiSi-type structure are naturally located close to the empirical Hill's criterion[98, 99]. However, much less attention has been paid to the other TiNiSi-type structure compounds particularly the isostructural and isoelectronic UIrGe, which has an antiferromagnetic (AFM) ground state (Néel temperature T_N = 16.5 K)[94, 100] with γ = 16 mJ/molK^2[100] and still lies just next to the boundary of Hill's limit having almost the identical $d_{U\text{-}U}$ like FM SC URhGe[94]. At temperatures below T_N, FOMPTs have been observed at critical fields $\mu_0 H_c$ = 21 T and 14 T (at 2 K) applied along *b* and *c*, respectively[101]. These interesting findings qualitatively similar to the magnetic features of URhGe along the *b*-axis motivated us to perform series of systematic studies of UIrGe magnetism and its stability under influence of external parameters like high pressure, magnetic field as well as substitution of Ir site by neighboring isoelectronic elements Co and Rh creating FM SCs. Our results have revealed the complex aspects of magnetic phase transitions in AFM UIrGe summarized in the first constructed detailed *p-T*, *H-T*, and *x-T* phase diagrams.

2.2.1 Effect of high pressure and *p-T* phase diagram of UIrGe [P4]

In this part of the research, we have investigated the effect of hydrostatic pressure on the magnetism of UIrGe. The plot in Figure 2.8 suggests that the contraction of the unit cell volume and the parameter $d_{U\text{-}U}$ by the hydrostatic pressure may drive the UIrGe compound to a FM state and finally to the magnetic instability. In such a case, hydrostatic pressure should cause the closing of the AFM gap and the recovery of the high coefficient, which is rather low in comparison with the FM SCs[40]. We supposed that UIrGe may be a candidate material in which the superconductivity can potentially develop on the boundary of the AFM phase induced by hydrostatic pressure.

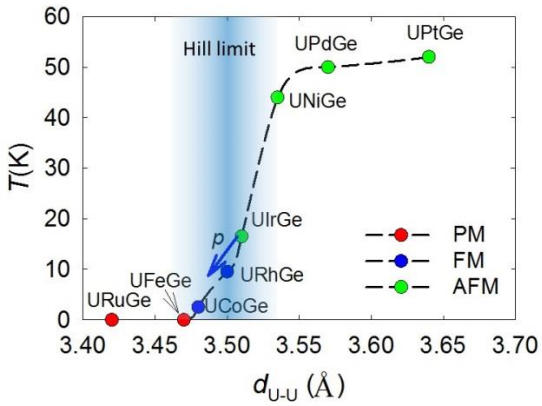

Figure 2.8 Evolution of magnetic ordering temperature and type in orthorhombic TiNiSi-type U*T*Ge compounds as a function of $d_{U\text{-}U}$. The blue arrow tentatively indicates the expected effect of hydrostatic pressure on the magnetism of UIrGe.

So far the best quality UIrGe single crystals were grown by Czochralski pulling in a tetra-arc furnace for the study, which was carried out in three types of pressure cells. A CuBe/NiCrAl piston-cylinder-type high-pressure cell was utilized up to ~1.7 GPa[102]. Experiments up to 15 GPa were performed in a cubic-anvil cell in The Institute for Solid State Physics, The University of Tokyo. Technical details are available in Ref.[103].

The preliminary experiment in the piston-cylinder type cell at pressures up to 1.7 GPa revealed a very small shift of the ordering temperature from T_N = 16.6 K at ambient

pressure to 16.4 K at 1.7 GPa. Nevertheless, it is a well-known fact that the response of physical quantities to external parameters is often nonmonotonic and a sudden change can appear approaching p_c[82, 104]. Therefore, we extended the hydrostatic pressure range up to 15 GPa using the cubic anvil cells. The value of T_N is only moderately affected up to 7 GPa. Then the T_N has started to drop up to 11 GPa to value 11.5 K. We did not find any evidence of a magnetic transition at 13 and 15 GPa. This suggests a sudden fall of T_N between 11 and 13 GPa. We collected the values of T_N from all the performed measurements and constructed the first *p*-*T* phase diagram Figure 2.9). As the diagram shows, we did not detect any sign of SC in the vicinity of the p_c down to 20 mK.

We conclude that the magnetism of UIrGe can be suppressed by hydrostatic pressure like in the case of FM UCoGe. However, the shapes of their magnetic domes are markedly different. The steep-like drop to zero from a relatively high T_N just above p_c in UIrGe is in contrast to the gradual vanishing of the FM in UCoGe up to the intersection with the summit of the SC dome[91, 97, 105]. The sudden drop in T_N at p_c and the resulting rectangular *p*-*T* phase diagram of UIrGe have the signature of a first-order transition. We surmise the scenario of a first-order transition based on the magnetic structure. The reported AFM magnetic structure of UIrGe consists of canted FM chains along the *a*-axis that are mutually antiferromagnetically coupled[106]. The FM chains along the *a*-axis in UIrGe are identical to the magnetic structure of the FM SC UCoGe[59, 69, 72], and URhGe[107].

We can deduce that there are two magnetic interactions in UIrGe, antiferromagnetic inter-*J*- and FM intra-*J**-chain interactions competing with each other. The *J** has the same nature as that in FM compounds. The pressure may affect the *J*-*J** balance in UIrGe and make the FM component more important at p_c. However, a high-pressure neutron diffraction experiment is highly desirable to resolve the magnetic structure of UIrGe in the vicinity of p_c to reveal the origin of the first-order-like transition that appeared in the recently reported *H*-*T*[83, 108] and *p*-*T*[109] phase diagrams of clean FM metals.

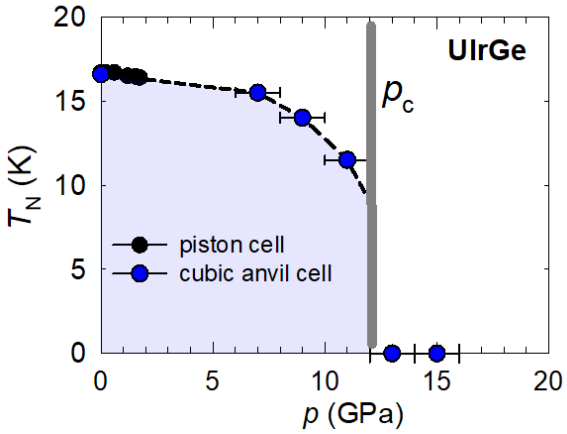

Figure 2.9 The *p*-*T* phase diagram of UIrGe. The grey line tentatively marks the critical pressure p_c.

The electrical resistivity data indicates moderately enhanced electron effective mass in the paramagnetic state above p_c. A Kadowaki-Woods empirical analysis gave reasonable agreement between the evaluated parameters *A* and γ below and also above p_c. Both quantities change abruptly at p_c. This corroborates the scenario that a rather large AFM gap is closed at p_c which may cause a large reconstruction of the Fermi surface and an increase of the Sommerfeld coefficient γ from its low value at ambient pressure.

We have also considered whether hydrostatic pressure can induce the AFM to FM transformation because of the reduced volume and the decrease in of $d_{U\text{-}U}$ upon applying pressure. The effect of the collapse of the AFM state followed by the development of a FM phase was recently observed in USb_2[104]. However, we did not have any evidence from the high-pressure electrical resistivity data that this occurs for UIrGe. This scenario contradicts the existence of a FM phase in lattice-expanded UIrGe hydride[110]. The FM in UIrGe can be drawn by the alloying with smaller Si atoms creating a lattice contracted paramagnet UIrSi[111, 112]. The surprising analogy between the hydrostatic and chemical pressure by Si substitution can be found in all three isoelectronic compounds. The response of UCoGe is similar to that of UIrGe[91, 97, 105]. Hydrostatic pressure increases T_C only in URhGe[113]. Accordingly, the Si analogs UCoSi[112] and UIrSi[111, 112] are paramagnets. URhSi is FM[76] with a higher T_C (10.5 K) than that of URhGe.

2.2.2 Effect of high magnetic field and *H-T* phase diagram of UIrGe [P5]

The motivation for the study of the *H-T* phase diagram of the UIrGe is the effect on the magnetic and superconducting properties of the neighboring FM SCs URhGe and UCoGe. Particularly in the case of URhGe, the field applied along the magnetically hard *b*-axis induces a reorientation of the U magnetic moments from the magnetization easy *c*-axis to the *b*-axis at a field H_R ~12 T[79, 83]. The ferromagnetic phase vanishes at H_R by a first-order transition and tricritical fluctuations [83, 84, 108, 114] accompanied with a Fermi surface reconstruction[88, 115, 116].

UIrGe is AFM but it also exhibits field-induced metamagnetic jump at ~21 T (at 4.2 K)[101, 117] along the *b*-axis, which qualitatively resembles the magnetic anomaly observed in URhGe. Moreover, a broad maximum at T_{max} = 29 K far above the magnetic ordering temperature (16.5 K) appears in the temperature dependence of susceptibility χ, which resembles the observations on the magnetization of UCoGe[78].

We have investigated high-quality UIrGe single crystal within the entire *H-T* phase space for magnetic field applied along the *b*-axis by detailed magnetization, specific heat, and magnetocaloric effect measurements in pulsed fields up to 60 T in The Institute for Solid State Physics at The University of Tokyo.

The collection of characteristic parameters of magnetism in UIrGe – T_N, H_c, T_{max}, H_m, and T_{dev} determined by the aforementioned measurements enabled us to construct a magnetic *H-T* phase diagram in the plane for magnetic fields along the *b* axis, which is displayed in Figure 2.10.

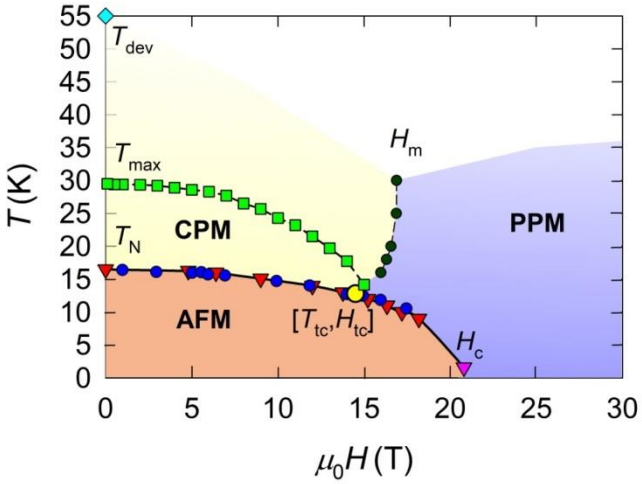

Figure 2.10 The UIrGe *T-H* phase diagram for magnetic fields applied along the *b* axis. The red triangles represent the H_c values of MTs determined by measurements of *M(H)* isotherms in static magnetic fields. The magenta triangle corresponds to H_c of the MT

detected at 1.6 K by the specific heat measurement in pulsed fields. The average of $H_{c\uparrow}$ and $H_{c\downarrow}$ values is displayed as H_c in the case of FOMPTs. The dark blue circles represent the T_N determined from $C_p(T)$ data in static magnetic fields reported in Refs[101, 118]. The dark green circles correspond to H_m values from pulsed-field $M(H)$ data. The green squares represent the T_{max} values, temperatures of maxima of $\chi(T)$ dependences measured in static magnetic fields. The yellow circle with coordinates $[T_{tc},H_{tc}]$ is the point between the low-temperature region with FOMPT and high-temperature region SOMPT. The light blue diamond corresponds to the temperature T_{dev}, below which the $\chi(T)$ data deviate from the high-temperature data (> 55 K) fit to an MCW law.

The phase diagram consists of the dome of the AFM phase, however, the MTs and field-induced magnetic states are rather complex. The MTs at T < 13 K and corresponding fields $\mu_0 H$ > 15 T exhibit a field hysteresis, a hallmark of FOMPT, whereas the transitions at higher temperatures T > 13 K and lower magnetic fields $\mu_0 H$ < 15 T show no trace of hysteresis as expected for SOMPT. The conclusion about FOMPTs at temperatures below 13 K is also corroborated by observing the asymmetric signal of the MCE observed in the vicinity of the transition. Moreover, the FOMPTs at low temperatures (<13 K) are accompanied by a dramatic increase of the Sommerfeld coefficient which is presumably a result of the Fermi surface reconstruction.

The extra S-shape curvatures have been detected at temperatures T > 13 K in the magnetization isotherms. The magnetic field H_m marking the inflection point of the S-shaped is attributed to the characteristic field of the crossover from the CPM to the PPM regime. The crossover line is heading towards the point, where the MT turns from the first-order to the second-order phase transition. T_{max} simultaneously approaches T_N to become equal $T_{max} \approx T_N$ at the tentatively considered TCP that separates the high-temperature segment of the SOMPTs and the low-temperature segment of the FOMPTs. Interestingly, also the line representing the temperature-induced evolution of H_m is bound for this point in the magnetic phase diagram.

To circumscribe properly the CPM regime we have established a characteristic temperature T_{dev}. When decreasing temperature below T_{dev}, the $\chi(T)$ data progressively deviate downwards from the MCW law, show a broad maximum at $T_{max,}$ and suddenly drop at T_N due to the onset of AFM ordering. The evolution of susceptibility correlates with the convex shape of magnetization curves between H_c and H_m. An effect of (dynamic) AFM correlations between magnetic moments (or static short-range AFM order) in the paramagnetic state may be tentatively considered as a possible explanation. The AFM correlations (or static short-range AFM order) may cause that some originally paramagnetic moments to couple antiferromagnetically with their counterparts.

The C_p/T value at 1.6 K, which can be in our case a reasonable estimate of γ, undergoes a sudden jump in the vicinity of H_c, when magnetic ordering is destroyed by the magnetic field. The C_p/T is stabilized at ~90 mJ/molK^2 above H_c, which corresponds to the extrapolated C_p/T (0 T) value from temperatures above T_N (0 T)[94]. We tentatively attribute this result to Fermi surface (FS) reconstruction although we are aware that also some other mechanisms, e.g. field-induced change of magnetic fluctuations, can cause the change of γ.

We concluded that UIrGe magnetic features are complex and qualitatively resemble the magnetic phenomena of FM SCs. The FOMPT and TCP were detected both in the phase H-T diagram of URhGe and UIrGe. Moreover, the FOMPT to PPM in UIrGe is connected with the recovery of high γ likely connected with Fermi surface reconstruction. On the other hand and in contrast to URhGe, the large area of the CPM region is detected above the AFM dome and its TCP. It may resemble the feature of

UCoGe, where a similar CPM region was detected. However, the CPM region in UCoGe *H-T* phase diagram fully covers the dome of FM in the *H-T* phase diagram therefore the MT from ordinary magnetic state to PPM cannot be realized.

2.2.3 Magnetism and phase diagram of $URh_{1-x}Ir_xGe$ system [P6]

The previous studies of UIrGe compounds and revealed similarities of the magnetic phenomena with FM SCs UCoGe and URhGe motivated us to focus on how the ferromagnetic state of FM SCs will transform to AFM state of UIrGe. We have utilized the fact that the UIrGe[119] has an almost identical parameter $d_{U\text{-}U}$ with URhGe. In this part of the research, we have studied the magnetic properties in the substituted pseudoternary $UIr_{1-x}Rh_xGe$ system where the FM/AFM boundary at low temperature is expected. Many studies have been carried out to determine the delicate balance of magnetic interactions in U*T*Ge alloy systems but primarily on polycrystalline samples where the features of magnetocrystalline anisotropy remain hidden[47, 52, 99, 120-123]. Our single crystal study has allowed us to develop a general picture of the magnetism in the AFM part of the $UIr_{1-x}Rh_xGe$ system which surprisingly preserves many of the magnetic features of the FM parent compounds URhGe and UCoGe. Our discussion and conclusions are based on a detailed analysis of the crystal structure, magnetization, and specific heat.

High-quality single crystals were grown by Czochralski pulling in a tetra-arc furnace from polycrystalline precursors of representative concentrations covering appropriately the full x scale of the $UIr_{1-x}Rh_xGe$ system. The AFM/FM boundary in the $UIr_{1-x}Rh_xGe$ system is interesting from the standpoint that AFM UIrGe and FM URhGe have very similar lattice parameters arising from almost identical radii of the transition element ions[124]. The unit cell volume of UIrGe is only about 0.07 % larger than that of URhGe[119, 125]. The very small change of the unit cell volume arises from the nearly perfect cancelation of the weakly expanded lattice parameter c and shortened b. The crucial parameter a remains unchanged and reflects an almost constant $d_{U\text{-}U}$ distance.

We have collected magnetic parameters of all the studied compounds in the $UIr_{1-x}Rh_xGe$ system and constructed a magnetic phase diagram (Figure 2.11).

The fundamental result is the detected discontinuity in all magnetic quantities between the utmost AFM $UIr_{0.45}Rh_{0.55}Ge$ and FM $UIr_{0.43}Rh_{0.57}Ge$. We have detected the discontinuity in the ordering temperatures as well as in $H_{b,crit,}$ and a finite value of $H_{c,crit}$ on the AFM side. The discontinuity between the FM and AFM at critical concertation ~$UIr_{0.44}Rh_{0.56}Ge$ is also supported by the specific heat of AFM $UIr_{0.45}Rh_{0.55}Ge$ with the nascent FM phase with no sign of a merger of T_C and T_N. Instead, a clear gap ~2.3 K was detected. A particularly important issue is the evolution of the maximum in magnetic susceptibility at T_{max}. It is an intriguing property of URhGe where $T_C \approx T_{max}$[78, 88] and this trend is maintained towards the ultimate FM compound $UIr_{0.43}Rh_{0.57}Ge$. T_{max} suddenly splits from T_N at the AFM border.

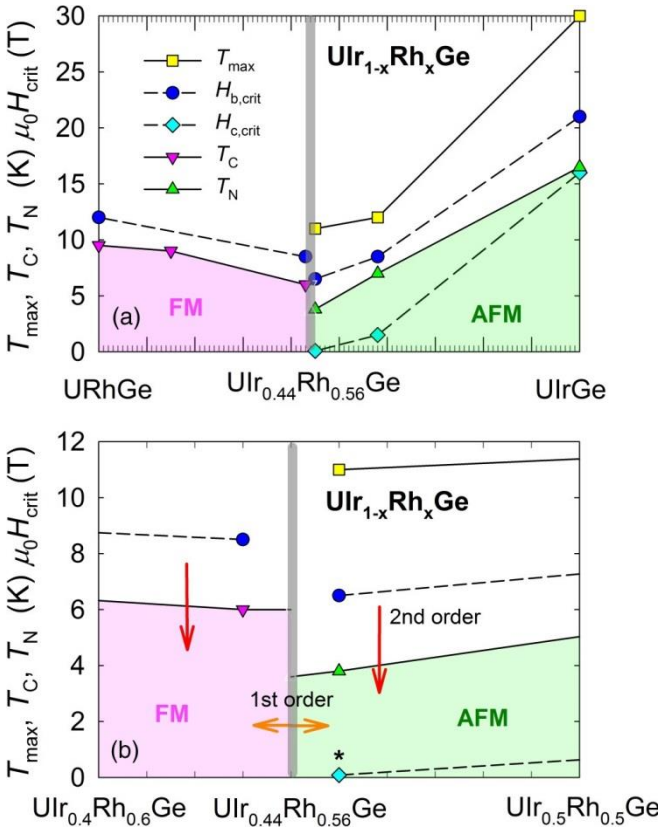

Figure 2.11 Magnetic phase diagram of the $UIr_{1-x}Rh_xGe$ system. The upper panel shows the full concentration range, the bottom one shows the area around the AFM/FM boundary in detail. *The point is 0.085T. The critical concentration is tentatively established at $x_{crit} = 0.56$. The lines are guides to the eye.

At the FM/AFM boundary, both the T_N and T_C are finite. Such a phase diagram could be realized in a system involving two independent magnetic intra- (J) and inter- (J^*) chain couplings along the axis a. Indeed, U moments are aligned ferromagnetically along the chain in both UIrGe and URhGe. This indicates $J > 0$ (FM) on both sides of the boundary. Then the AFM/FM boundary can be defined as the point where only J^* changes sign from $J^* < 0$ (AFM for Ir) to $J^* > 0$ (FM for Rh). Because of the discontinuous transition $J^* \neq 0$. Naturally, both T_N and T_C are finite with $J > 0$.

The second scenario considers the effect of bandwidth W_d of the valence 4*d* and 5*d* states of Rh and Ir[126], respectively, affecting the 5*f*-*d* hybridization and also the spin-orbit *s*-*o* interaction of the much heavier Ir ion[127]. This should be verified by a detailed electronic structure study by ARPES or dHvA effect in UIrGe.

Existence of the quantum critical points QCP was reported in the neighboring alloying FM-PM and AFM-PM systems $URh_{1-x}Ru_xGe$[51, 128], $UCo_{1-x}Fe_xGe$[56], $UCo_{1-x}Ru_xGe$[99] or $UPd_{1-x}Ru_xGe$[120]. The $UIr_{1-x}Rh_xGe$ system behaves like the other AFM-FM alloy system $UPd_{1-x}Co_xGe$ where magnetic order survives in the entire concentration range[121]. In contrast to $UPd_{1-x}Co_xGe$, a deep local minimum in the ordering temperatures is created at the AFM/FM boundary in $UIr_{1-x}Rh_xGe$ almost at the level of T_C of UCoGe. Secondly, the analysis suggests here an enhancement of the coefficient $\gamma_{UIr0.43Rh0.57Ge} \approx$ 175 mJ/molK^2 (Fig. 12), the highest in the UCoGe-URhGe-UIrGe system, indicating enhancement of the magnetic fluctuations typical for the development of a QCP reported in the above-listed alloy systems. However, magnetic fluctuations are interrupted in UIr_{1-}

$_xRh_xGe$ by a very stable AFM phase and a QCP is not due to the AFM gap opening in the magnetic Brillouin zone.

The constructed phase diagram opens the question of whether the *b*-axis crossover region circumscribed by T_{max} and H_m is a product of the specific feature of the uranium magnetism or it is related to a heavy-fermion phase. It seems that the crossover region is substantially reduced or does not exist in the URhGe because of $T_{max} \approx T_C$. Then, critical field $H_{b,crit}$ and T_{max} and T_C are proportional to a constant factor $H_{b,crit}/T_{max} = H_{b,crit}/T_C \approx 1.33$. On the other hand, we surmise a large area of the crossover region existing between the UCoGe - ~$UCo_{0.6}Rh_{0.4}Ge$ where $T_{max} > T_C$. Very high $H_{b,crit} \sim 50$ T of UCoGe seems to be connected with T_{max} not having any relation with T_C. Identically, the $T_{max} > T_N$ in the AFM $UIr_{1-x}Rh_xGe$ but both seem to have one common $H_{b,crit}$. Thus, the relation between T_C, T_N, T_{max} and $H_{b,crit}$ varies through the system and is digestedly summarized in Figure 2.12.

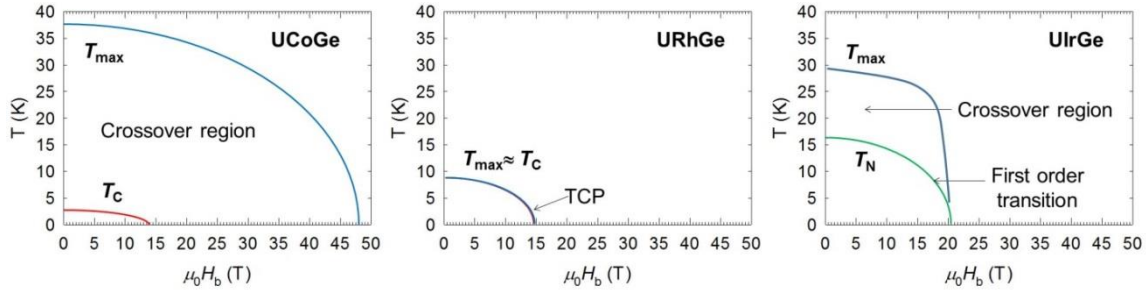

Figure 2.12 Schematic H_b-T phase diagrams of the UCoGe, URhGe, and UIrGe. The UCoGe diagram was constructed using data from works[78, 129], URhGe diagram from work[78], and UIrGe using our data and work[101]. The position of the TCP in URhGe was taken from work[83]. The transformation from the SOMPT to FOMPT in UIrGe was deduced from the specific heat data in work[101].

We conclude that $UIr_{1-x}Rh_xGe$ system represents a discontinuity at $x_{crit} = 0.56$ in all the magnetic parameters between the FM and AFM phase typical for the first-order transition. QCP is not realized at x_{crit} because of finite T_C and T_N. However, magnetic fluctuations are moderately enhanced approaching the FM limit. The recovery of the magnetic fluctuations in the AFM compounds is possible in an applied magnetic field along the *b*- and *c*-axis. Stronger fluctuations are expected along the *b* axis probably due to the crossover region.

2.2.4 Magnetism in $UCo_{1-x}Ir_xGe$ system [P7]

It is, of course, of natural interest to see the effect of alloying UIrGe with the second FM superconductor UCoGe. The evolution of magnetism with increasing distance of U nearest neighbors within the series of UTGe compounds seems to follow Hill's scenario [40, 99, 130] when starting by the paramagnetic (PM) ground state of URuGe followed up by ferromagnets UCoGe[32] and URhGe[131] and antiferromagnets (AFM) UIrGe[93, 101], UNiGe[132-134] and UPdGe[48, 49]. Despite this empirical finding, the evolution of magnetism in pseudo-ternary alloy systems is often unexpectedly different as it was shown in the previous$UCo_{1-x}Ru_xGe$, $UCo_{1-x}Rh_xGe$, and $URh_{1-x}Ir_xGe$ systems. This confirms the fact that the microscopic origin of the magnetism in these compounds is more complex than determined only by the overlaps of the 5*f* orbitals of the nearest-neighbor U ions. We could see that despite this empirical finding, the evolution of

magnetism in pseudo-ternary alloy systems is often unexpectedly different. This confirms the fact that the microscopic origin of the magnetism in these compounds is more complex than determined only by the overlaps of the 5*f* orbitals of the nearest-neighbor U ions. The strong role of competing FM and AFM interactions mediated by the 5f-ligand hybridization determining the magnetic ground state was predicted for these compounds[92, 135].

These aspects motivated us to investigate the $UCo_{1-x}Ir_xGe$ system which has a ferromagnet (UCoGe) and an antiferromagnet (UIrGe) as parent compounds. The FM intra-chain coupling is preserved in both mother compounds. On the other hand, the AFM inter-chain coupling of U magnetic moments is present in UIrGe [136]. Moreover, the UCoGe exhibits uniaxial magnetocrystalline anisotropy with the easy magnetization axis along the *c* direction while an XY-type anisotropy with the easy *bc*-plane has been reported in UIrGe. The strong role of competing FM and AFM interactions mediated by the 5f-ligand hybridization determining the magnetic ground state was expected in this system.

To study the development of the magnetic states in the $UCo_{1-x}Ir_xGe$ system we have prepared a series of polycrystalline samples with different Co/Ir concentrations to fully cover all regions of expected interesting magnetic property changes. Based on the polycrystalline study several single crystals were grown by Czochralski pulling in a tri-arc furnace using pulling speeds of 6 mm/h.The magnetization, specific heat, and resistivity data allow us to sketch a tentative *T*-*x* magnetic-phase diagram for the $UCo_{1-x}Ir_xGe$ system shown in Figure 2.13. The AC susceptibility and electrical resistivity measurements down to 0.4 K revealed that the superconductivity persist only up to $x = 0.01$.

The resulting *T*-*x* phase diagram of the $UCo_{1-x}Ir_xGe$ system is characterized by a very narrow concentration interval of stability of ferromagnetism and a wide intermediate concentration region without magnetic ordering. This contrasts the evolution of magnetism in the $URh_{1-x}Ir_xGe$ system reported to exhibit an extended range of stable ferromagnetism in Rh rich compounds up to a discontinuous transformation (typical for a first-order transition) between the FM and AFM phases of parent compounds at a critical concentration $x_{crit} = 0.56$ [135].

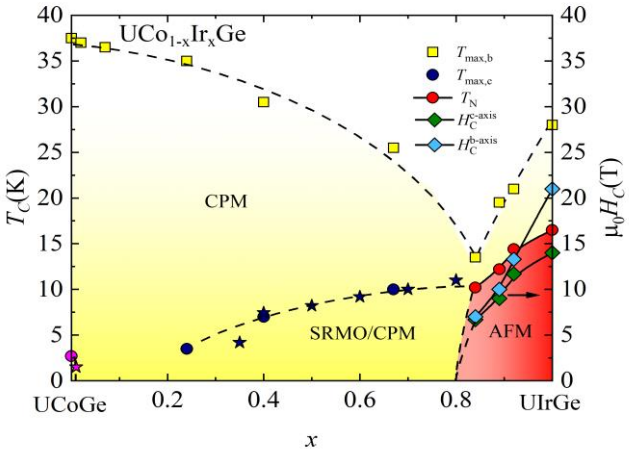

Figure 2.13. *T*-*x* magnetic phase diagram of $UCo_{1-x}Ir_xGe$ system. The temperatures marked by magenta/navy stars depicting $T_C/T_{max,c}$ were obtained on polycrystals. The data for UCoGe (marked by a magenta circle) are taken from Ref.[137].

Finding a plausible explanation for the striking difference between the *T*-*x* phase diagrams of $UCo_{1-x}Ir_xGe$ and $URh_{1-x}Ir_xGe$ is not an easy task. We can try to approach this

problem by discussing the mechanisms affecting the key components of magnetism in uranium intermetallic compounds, uranium magnetic moments, and exchange interactions between them with a special focus on the studied systems.

The 5*f*-electron uranium wave functions, which are propagated in space overlap and interact with the 5*f*-orbitals of neighboring U ions (5*f*-5*f* overlap) and hybridize with valence electron orbitals of nonuranium ligands (5*f*-ligand hybridization)[138]. As a result, the 5*f*-orbitals lose in compounds their atomic character and the U magnetic moments are reduced compared to free U-ion moments (U^{3+} or U^{4+}). The large 5*f*-5*f* overlap by rule prevents the formation of a permanent atomic 5*f*-electron magnetic moment in materials in which the distance of nearest-neighbor U atoms (called $d_{U\text{-}U}$) is smaller than the Hill limit[7]. The 5*f*-ligand hybridization has more subtle effects on magnetism which show up in the lower U-content compounds where the ligands surrounding U ions prevent the direct U-U bonds[138]. The direct overlap of U 5*f* -wave functions is also responsible for the direct U-U exchange interaction, while the 5*f*-ligand hybridization mediates the indirect exchange interaction between U ion moments separated by the involved ligand.

The strong spin-orbit interaction in uranium ions induces an orbital magnetic moment that dominates the spin moment. This happens in all so far investigated magnetic U materials even in the cases of weak itinerant ferromagnets like UNi_2[139, 140] and UCoGe[69, 141].

The ferromagnetism in UCoGe is characterized by the low T_C value (= 2.7 K) and an extremely reduced spontaneous magnetic moment μ_s = 0.07 μ_B at 2 K[142]. The ferromagnetic ordering in UCoGe is suppressed by the application of low hydrostatic pressure of only ≈ 1 GPa[91, 97, 105]. The small magnetic moment and rapid suppression of T_C in hydrostatic pressure are hallmarks of weak itinerant ferromagnetism.

URhGe becomes ferromagnetic at higher T_C (= 9.6 K) and the magnetic moment of $\mu_s \approx 0.4$ μ_B is also reduced but still much larger than that in UCoGe[131, 143]. Results of electronic structure calculations for URhGe[144] suggest itinerant *5f*-electron ferromagnetism also in this compound. However, the ferromagnetic order in URhGe is unusually stable in applied hydrostatic pressure. The Curie temperature increases with linearly increasing applied pressure up to ≈ 17.5 K at 13 GPa[145].

The increase of T_C with pressure in metallic ferromagnets is usually associated with more localized magnetic states, i.e. 5*f*-electron states in U compounds. UGa_2 can be taken as a prominent example[146, 147]. Very different degrees of localization can be identified e.g. by the response of critical temperature to external pressure. It has been demonstrated by an opposite pressure effect on T_C in the ferromagnets, namely a negative effect in the case of UCoGa with more delocalized 5*f* states and positive effect in URhGa having the 5*f* states considerably more localized leading to much larger U magnetic moments than in the UCoGa case[145, 148], represents an analogy to the pair UCoGe, URhGe. In this scenario, the UCoGe is a weak itinerant 5*f*-electron ferromagnet with the spontaneous moment of 0.07 μ_B/f.u. and URhGe has considerably more localized 5*f*-electron states yielding a stable U moment of 0.43 μ_B/f.u. This is also well documented by the stability of ferromagnetism in $URh_{1-x}Ir_xGe$ which persists up to x = 0.43 whereas the ferromagnetism in $UCo_{1-x}Ir_xGe$ ceases with only slight Ir doping of $x < 0.02$. A tiny U magnetic moment in UCoGe appears on the verge of instability. It is known that no ferromagnetic order could be observed in some UCoGe samples[41, 149]. Therefore the substitutional disorder in $UCo_{0.98}Ir_{0.02}Ge$ could be considered as the mechanism suppressing the ordered U moment[148, 150, 151].

Important arguments corroborating the very different degree of localization of 5*f*-electrons and consequently the different stability of ferromagnetism in UCoGe and URhGe provide the values of lattice parameters. The URhGe unit cell is apparently in all

three dimensions larger than that of UCoGe. This implies also a larger value of d_{U-U} and other interatomic distances leading to a smaller 5*f*-5*f* overlap and weaker 5*f*-ligand hybridization, which results in a less reduced U magnetic moment in URhGe. UIrGe and URhGe have very similar lattice parameters arising from almost identical radii of the transition element ions[124]. Thus, the changes in lattice parameters due to substitutions in the $URh_{1-x}Ir_xGe$ system are almost negligible. Then stable FM and AFM phases on the Rh and Ir side, respectively, of the phase diagram can be expected.

3 UTX of ZrNiAl structure type

Besides the ternary UTX orthorhombic compounds of TiNiSi-type structure, there is another large group of hexagonal compounds of identical formula crystalizing in the ZrNiAl structure type. The typical p-elements in these series are Sn, Al, Ga, and In. While the U ions are arranged in the zig-zag chain in TiNiSi-type compounds, ZrNiAl is a layered structure where mixture layers of U-T ions are periodically stacked with the T-X layers. This structural arrangement and strong overlap of the U 5f wave functions within the U-T layers are responsible for strong magnetocrystalline anisotropy of these compounds with magnetization easy axis typically along the hexagonal c-axis. The resulting two unique T-metal sites in ZrNiAl are another difference in contrast with the TiNiSi-type structure compounds[152]. A large variety of magnetic ground states can be found in this class of compounds from the rank of PMs, FMs as well as AFMs with complex magnetic structures[153, 154]. The recent interest focuses on ground state PM UCoAl[63, 155-159] which features differ significantly from ordinary PMs. UCoAl has attracted much interest because of the very low critical field of the MT ($B_c \approx 0.6$ T), which occurs only in fields parallel to the *c* axis[160] accompanied by tricritical phenomena[161-163].

3.1 Magnetism and magnetic phase diagram of $UCo_{1-x}Ru_xAl$ [P8]

A spectacular feature of the PM UCoAl is the rise of very stable FM in its solid solutions already at tiny concentration of dopant (x < 1%). The observed sudden FM in UCoAl is a surprisingly general phenomenon for the majority substituting *T*-metals. The $UCo_{1-x}Ru_xAl$[164] solid solutions, the subject of our research, is the case where the FM phase rises between two ground state PMs[165]. Already the tiny amount of Ru ($x \approx 0.01$) in UCoAl suddenly gives rise to stable FM with an enormous T_C jump from zero up to almost 20 K[166, 167]. Further substitution by Ru increases T_C reaching 60 K for $x \approx 0.3$. Beyond this optimum amount, the FM phase is suppressed and survives up to the critical Ru concentration $x_{crit.} \approx 0.8$. However, the later FM phase behavior significantly changes at higher concentrations[166, 168-171]. Since the features of the FM phase differ at opposite boundaries, it indicates the evolution of the magnetic interactions through the system. While FOMPT is predicted for the clean FM metals SOMPT FM/PM transitions can extend down to 0 K in disordered metals[172]. Thus, $UCo_{1-x}Ru_xAl$ represents a unique system for research where FM QCP can appear in both limits of substitutional disorder – in the limit of a clean FM metal (UCoAl side of the FM dome) and disordered FM metal (URuAl side of the FM dome). Moreover, the microscopic relation of the strong FM in $UCo_{1-x}Ru_xAl$ to particular properties of the parent PM compounds was unclear.

For the study, $UCo_{1-x}Ru_xAl$ single crystals with nominal compositions $x = 0.60$, 0.73, and 0.81 were grown by the Czochralski method in tri-arc and tetra-arc furnaces and investigated by mean of magnetic transport, thermodynamic methods. The

microscopic origin of magnetism was investigated by neutron diffraction. The polarized neutron diffraction experiments were performed on the same sample on the 5C1 diffractometer at the LLB Saclay institution.

Key results are provided by PND (Figure 3.1), showing the development of the hybridization strength through the system. Microscopic evidence for delocalization of the 5*f* states can be deduced from the value of the $|\mu_L^U/\mu_S^U|$ ratio. Generally, a higher value of $|\mu_L^U/\mu_S^U|$ suggests a stronger localization of the 5*f* electrons and vice versa[72, 74, 75]. Here, in the vicinity of $T_{C,max}$ for $UCo_{0.38}Ru_{0.62}Al$, $|\mu_L^U/\mu_S^U|$ equals only 1.63(12) which is far from the U^{3+} and U^{4+} free ion values[72] and comparable to that seen in the generally accepted itinerant FM UCoGe[69, 72, 141]. $|\mu_L^U/\mu_S^U| \approx 2.3$ was found for the field induced FM state of UCoAl[62]. The URuAl magnetic ground state is rather unusual. Calculated band structure based on spin and orbital-polarized LSDA method supposes that PM state is caused by the almost perfect cancelation of the reduced μ_L^U and μ_S^U resulting $|\mu_L^U/\mu_S^U|$ ratio only 1.3[165]. $|\mu_L^U/\mu_S^U| = 1.63$ of $UCo_{0.38}Ru_{0.62}Al$ is in between that of UCoAl and that expected for URuAl.

The strength of the hybridization can be deduced from the proportion of the induced magnetic moments in *T* - sites. While almost equivalent induced magnetic moments were found in Co sites in UCoAl[62] the Ru sites in URuAl are magnetically inequivalent with the significantly larger magnetic moment in the U - *T* plane[65]. Our results show two times higher induced magnetic moment for *T* site in U - *T* plane. It gives evidence for the growth of the hybridization strength in U - *T* plane most likely driving the magnetism in $UCo_{1-x}Ru_xAl$. It is in agreement with the observation by Hall effect. ρ_H of $UCo_{0.38}Ru_{0.62}Al$ is similar to UCoAl at the metamagnetic transition[156]. Significantly enhanced values of ρ_H were detected for $UCo_{0.25}Ru_{0.75}Al$ and $UCo_{0.24}Ru_{0.76}Al$, which agree well with the suggested importance of seven *d* electrons for the paramagnetic state of URuAl[165]. Nevertheless, we did not find any scaling of the magnetic parameters in the ZrNiAl-type U*T*Al FMs representing more complex magnetic interactions in comparison to neighboring TiNiSi-type U*T*X FMs (with one unique *T* site) where scaling of S_{mag} and $|\mu_L^U/\mu_S^U|$ were found for a large series of pure and also substituted compounds as the functions of $d_{U\text{-}U}$ and T_C[72, 99].

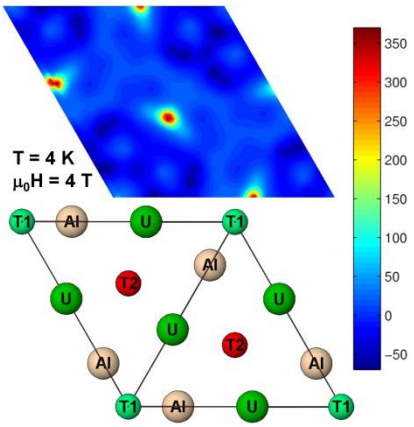

Figure 3.1 Magnetization density map of the $UCo_{0.38}Ru_{0.62}Al$ in basal plane. The red shade represents the atoms in the T-Al layer, green shade U-T layer. The scale of the map is in $m\mu_B$ unit.

Based on analysis of all experimental data, we have estimated $x_{crit.} \approx 0.77$ where FM phase vanishes (Fig. 10). Our previous conclusions show that hybridization strength

develops gradually with increasing x. In contrast, the FM dome is markedly asymmetric at the boundaries. More rapid change of T_C (~20 K / 1 % Ru) is seen on the UCoAl side[166, 167] than that (~ -3 K / 1 % Ru) on the URuAl side. It is known that in clean FMs original second-order transition transforms to the first order at TCP by tuning of the critical parameter[172]. It was recently confirmed in FM URhAl[109]. With increasing disorder, the temperature of the TCP decreases, and above a critical disorder strength, a QCP is realized in zero temperature. In agreement, Ru (and many other T metals) substitution causes instantaneous transformation of the metamagnetic UCoAl to the FM state[167] and transition changes from first- to second- order. Then, FM is established at the temperature where the original spin fluctuations appear. The scenario was confirmed by NMR in neighboring $UCo_{1-x}Fe_xAl$[158, 163, 173]. We expect the existence of a TCP in $UCo_{1-x}Ru_xAl$ around 1% of Ru Figure 3.2.

On the opposite side of the FM dome near $x_{crit.}$, there is no evidence for the first-order transition and electrical resistivity exponent drops from $\sim T^{2.0}$ to $\sim T^{1.5}$ together with straightening of the C_{mag}/T on a logarithmic scale. It is evidence for approaching a QCP[51, 56, 99]. High x $UCo_{1-x}Ru_xAl$ alloys, however, show apparent differences from critical behavior of similar alloying systems[51, 56, 99]. Enhancement of the Sommerfeld γ coefficient is broad and very weak around $x_{crit.}$ and electrical resistivity starts to vary $\sim T^2$ already when T_C is still very high (18 K of $UCo_{0.30}Ru_{0.70}Al$). Wide region of the electrical resistivity exponent variation suggests that a finite critical region develops instead of a thermodynamic observables singularity.

Notable broadening of the critical region is predicted for Griffiths effect where a magnetically inhomogeneous phase develops in the disordered systems and FM/PM boundary smears due to so-called rare region[174, 175] (Fig. 10). These rare spatial regions are locally magnetic while the bulk is nonmagnetic. Characteristic parameters of the locally magnetic regions are their volume V depending on disorder strength and characteristic energy ε exponentially depending on V. Final energy spectrum is defined as $P(\varepsilon) \sim \varepsilon^{\lambda-1}$ where λ is the Griffiths exponent of which power-law spectrum gives singularity in many quantities[176]. Data analysis indicates that $UCo_{1-x}Ru_xAl$ features also fit the Griffiths scenario. Magnetic clusters within the rare region respond to the frequency of the modulation field in AC susceptibility together with a deviation of the magnetization measured in FC and ZFC regime which is in agreement with our observations.

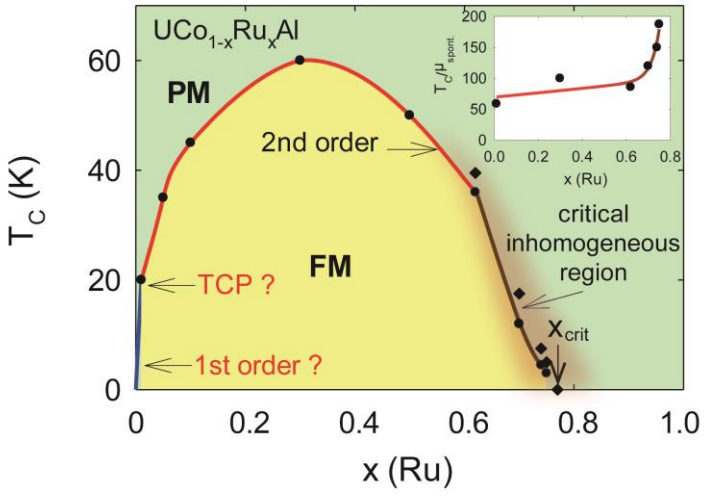

Figure 3.2 T-x phase diagram of the $UCo_{0.38}Ru_{0.62}Al$ system.

3.2 Ferromagnetism of URhAl [P9]

Itinerant FMs have attracted much attention because of their interesting physical properties, for example, unconventional superconductivity. In particular, many experimental and theoretical studies have looked at novel phenomena related to a quantum phase transition (QPT) between FM and OM states that can be tuned by external parameters. Novel features of the physical properties under high pressure and high magnetic field have been extensively studied for the ferromagnetic superconductors UGe_2, URhGe, and UCoGe, and strongly uniaxial ferromagnets UCoAl, Ru doped UCoAl, URhAl, and UCoGa[84, 97, 109, 155, 161, 177-179]. The line of continuous ferromagnetic transitions forms a "wing structure" in the temperature-pressure-magnetic field phase diagram of the uranium FMs. When the pressure is applied, the paramagnetic to ferromagnetic transition changes from a second-order to a first-order transition at TCP before the critical pressure of the FM state and the line bifurcates into finite magnetic fields at the TCP. Review papers give the current status of experimental and theoretical studies on this subject[10, 11].

Generally, the FM states in the uranium FMs are strongly uniaxial and experimental data are discussed with theories based on the 3D Ising model. The study of the critical behavior of the magnetization provides crucial information as to the type of the magnetic phase transition and nature of spin-spin interactions. The universality class of the critical phenomena in the uranium FM SCs UGe_2 and URhGe do not belong to any known universality classes of critical phenomena such as the 3D Ising model[180]. We suggest that uniaxial uranium ferromagnets have special features that cannot be understood only with the 3D Ising model. We report the critical behavior of the magnetization in URhAl.

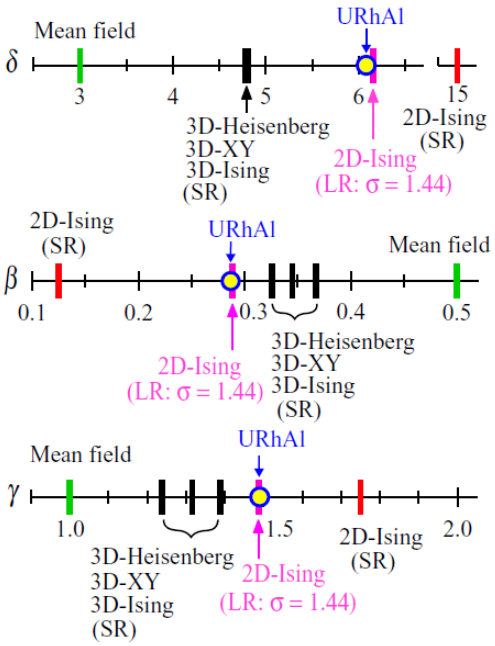

Figure 3.3 Comparison of the critical exponents β, γ, and δ in URhAl denoted as closed circles with those of known universality classes shown as vertical bars: mean-field, 2D-Ising, 3D-Ising,3D-XY, and 3D-Heisenberg models with short-range exchange interactions, and 2D-Ising model with long-range ($\sigma = 1.44$) interactions.

We have studied the critical behavior of the magnetization in uranium ferromagnet URhAl[181, 182] at around its ferromagnetic transition temperature T_C = 26.02 ± 0.02 K (Figure 3.3). The critical exponent β for the temperature dependence of the spontaneous

magnetization below T_C, γ for the magnetic susceptibility, and δ for the magnetic isotherm at T_C have been determined with a modified Arrott plot[183], a Kouvel-Fisher plot[184], the critical isotherm analysis, and the scaling analysis. The critical exponents have been determined as $\beta = 0.287 \pm 0.005$, $\gamma\_ = 1.47 \pm 0.02$ for $T < T_C$, $\gamma = 1.49 \pm 0.02$ for $T_C < T$, and $\delta = 6.08 \pm 0.04$ by the scaling analysis and the critical isotherm analysis. The obtained critical exponents satisfy the Widom scaling law $\delta = 1 + \gamma/\beta$. Although uniaxial magnetic properties in URhAl and its isostructural UCoAl has been discussed based on the 3DIsing model in previous studies, the universality class of the critical phenomenon in URhAl does not belong to the 3D Ising system ($\beta = 0.325$, $\gamma = 1.241$, and $\delta = 4.82$) with short-range exchange interactions between magnetic moments. The determined exponents match well with those calculated from the renormalization group approach for a two-dimensional Ising system coupled with long-range interactions decaying as $J(r) \sim r^{-(d+\sigma)}$ with $\sigma = 1.44$. We suggest that the strong hybridization between uranium 5*f* and rhodium 4*d* electrons in the U-Rh layer in the hexagonal crystal structure takes an important role in the low dimensionality of the critical phenomenon.

4 Magnetism of U_2T_2X

Compounds of composition $RE(A)_2T_2X$, (RE = rare-earth element, or A = actinide, T = transition metal, and X = p-element), crystallizing in the tetragonal Mo_2FeB_2 type of structure with space group *P4/mbm*[185], represent a large group, which has been intensively studied due to the extraordinary freedom to combine the various constituting elements while maintaining the structure type[186-188].

Uranium compounds display a large diversity of the types of the magnetic ground state, including itinerant PMs (U_2Co_2In, U_2Ru_2Sn), some with pronounced spin-fluctuation behavior (U_2Co_2Sn [189] and U_2Ir_2In[186]), suspected Kondo behavior (U_2Rh_2In[190]), and long-range AFM ordering (U_2Ni_2In, U_2Ni_2Sn, U_2Rh_2Sn, U_2Pd_2In, U_2Pd_2Sn, and U_2Pt_2Sn)[186, 191]. Some of the U_2T_2X compounds, like U_2Pt_2In[192] and U_2Pd_2In[188], exhibit heavy-fermion phenomena at low temperatures and signatures of geometrical frustration of the lattice and strong spin-orbit coupling[193, 194].

From the large series of U_2T_2X compounds, so far practically only In and Sn compounds have been systematically studied. The only Pb compound existing only in the polycrystalline form is U_2Pd_2Pb, which AFM at $T_N = 65$ K and undergoes an order to order transition at $T_1 = 20$ K[195].

Within new materials prospection, we have successfully prepared the first lead material U_2Rh_2Pb in the form of high-quality single-crystals of RRR = 97.

4.1 Magnetism and magnetic phase diagram in U_2Rh_2Pb [P10]

In the present study, we have described the synthesis, structure, and magnetic properties of U_2Rh_2Pb material. This compound was found interesting in several aspects It revealed strong magnetocrystalline anisotropy and constructed *H-T* phase diagram exhibits the lowest critical magnetic field of the field-induced MT transition among U_2T_2X compounds.

A series of needle-like U_2Rh_2Pb single crystals (Figure 4.1) has been grown by the self-flux method. The best results were obtained with the starting compositions U:Rh:Pb = 1:1:15 and 1:1:25. The shortest uranium-atom distance $d_{U\text{-}U}$ is within the U-atoms chain along the *c* axis and is identical to the lattice parameter *c*. This means that the critical distance $d_{U\text{-}U}$ in U_2Rh_2Pb is shorter than in the analog In and Sn Rh

compounds but still within the magnetic limit of the empirical Hill's criterion[7]. Details are described in the author's work[196].

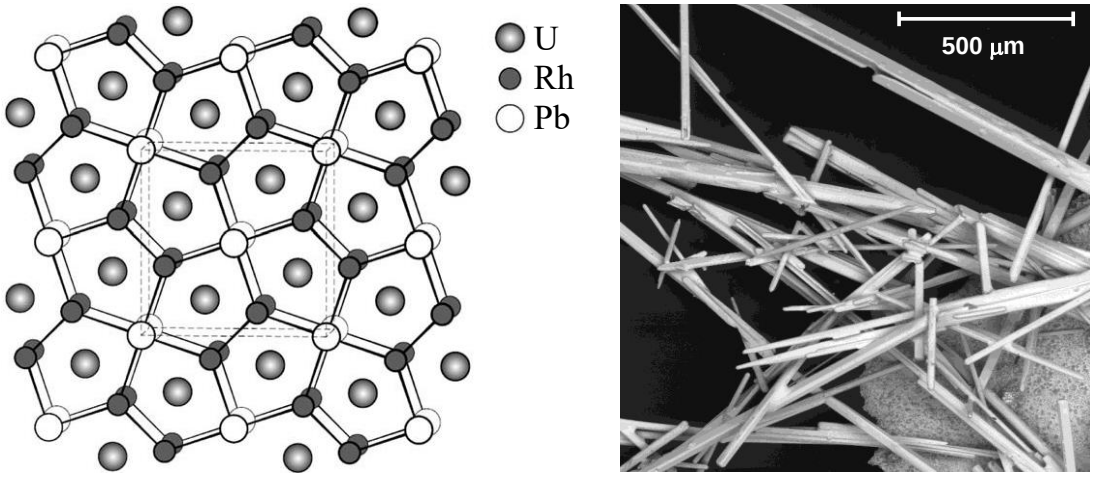

Figure 4.1 Crystal structure morphology of the U_2Rh_2Pb single crystals in a dense needle nest.

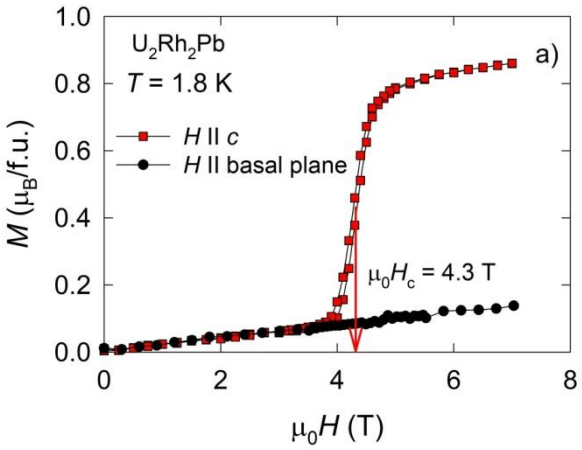

Figure 4.2 Magnetization isotherms of U_2Rh_2Pb measured at T = 1.8 K with the magnetic field parallel to the *c*-axis and parallel to the randomly oriented basal planes.

The *c*-axis orientation of U moments in U_2Rh_2Pb (Figure 4.2) is in contradiction with the tendency of uranium magnetic moments oriented due to the two-ion anisotropy perpendicular to the shortest $d_{U\text{-}U}$ distance[197, 198] which is along the *c*-axis in U_2Rh_2Pb. Following this rule, all the U_2T_2X compounds with the shortest $d_{U\text{-}U}$ along *c* have an easy-magnetization axis within the tetragonal basal plane[199, 200], and U_2Ni_2Sn with the shortest $d_{U\text{-}U}$ within the plane has the moments along *c*[198]. The only exception, U_2Rh_2Sn, which has also an easy magnetization direction along with *c*, can be perhaps explained by a strong hybridization between U 5*f* states and Rh 4*d* electron states [197, 198]. In this context, U_2Rh_2Pb with the *c*-axis U-U spacing 3% below the shortest U-U spacing in the basal plane is even more exceptional than U_2Rh_2Sn, where this difference is 2% at room temperature and 1% at low temperatures.

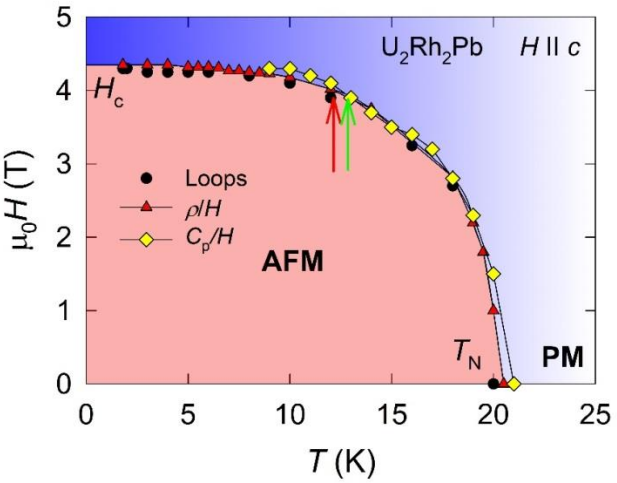

Figure 4.3 *H-T* magnetic phase diagram of U_2Rh_2Pb for *H* parallel to the *c*-axis. The red arrow indicates the temperature above which the hysteresis appears at MTs in the magnetoresistance. The green arrow indicates the field above which clear bifurcation of the FC and ZFC magnetization branches is detected.

The magnetic phase diagram of U_2Rh_2Pb for *H* along the *c*-direction constructed based on magnetization, electrical resistivity, and specific heat data is shown in Figure 4.3. The phase diagram of U_2Rh_2Pb is rather simple and consists of one magnetically ordered AFM phase. A special feature is the occurrence of AFM transitions with and without hysteresis. The temperatures above which the hysteresis and the bifurcation of the FC and ZFC magnetization curves disappear are indicated in the phase diagram by arrows. In previously studied AFM materials[93, 201, 202], the disappearance of the hysteresis has been considered as one of the signatures of a tricritical point (TCP) in the phase diagram which separates first- and second-order AFM transitions and exhibiting Ising-type anisotropy[202-206]. This supports the existence of TCP in U_2Rh_2Pb around T_{tc} = 13 K and $\mu_0 H_{tc}$ = 4 T. It should be pointed out that TCP is an inherent feature of a broad class of AFMs, in which the MT at low temperatures is of the first-order type and magnetic critical point in zero-field is of the second-order type, and hence does now imply any temperature variations of magnetic interactions[207]. A very unusual feature of MT in U_2Rh_2Pb is the observed value for $\mu_0 H_c$ = 4.3 T. So far the lowest among the AFM U_2T_2X compounds[186], for which the values of H_c are typically larger than 20 T and field-induced MTs may appear even above 60 T[208].

We conclude that we have prepared U_2Rh_2Pb a new member of the large series of tetragonal U_2T_2X (T – transition metal, X – Sn, In, Pb). It is AFM with T_N = 20 K with an unusually low value of $\mu_0 H_{tc}$ = 4.3 T of MT. The enhanced Sommerfeld coefficient γ of about 150 mJ/mol K^2 infers the presence of strong correlation effects however any clear signature of correlated regions was not detected in the phase constructed *H-T* phase diagram. The reduced magnetic-entropy change 0.3**ln*2 at T_N indicates the itinerant character of 5*f* electrons. The observed *c*-axis orientation of U magnetic moments is in contrast with the nearest U-U bonds along *c*, usually implying the basal-plane orientation. Magnetic phase diagram constructed for *H* parallel to the *c*-axis hints at the existence of a tricritical point around 13 K and 4 T.

5 Itinerant ferromagnetism of uranium compounds [P11]

Actinide compounds with 5*f* electrons have long attracted much attention because of their interesting magnetic and electronic properties such as heavy fermion features, unconventional superconductivity, the coexistence of the SC and magnetism, and physical phenomena associated with multipole degrees of freedom of the 5*f* electrons[17, 209-211]. Similar unusual physical properties have been extensively studied in other strongly correlated electrons systems such as oxides and organic and rare-earth compounds. It was necessary to reveal the behavior of the electrons responsible for these properties and find the universality of the electronic properties in the different systems. The peculiarities of the physical phenomena in actinide systems are ascribed to the role of the 5*f* electrons. In actinide metallic compounds, the degree of localization of the5*f* electrons differs in different compounds, ranging from strongly localized to the itinerant character. The 3*d* electrons in transition metals also show various degrees of localization. Differences between the 5*f* and 3*d* electrons are the smaller sensitivity to the crystal field from ligand atoms and the stronger spin-orbit coupling in the 5*f*'s.

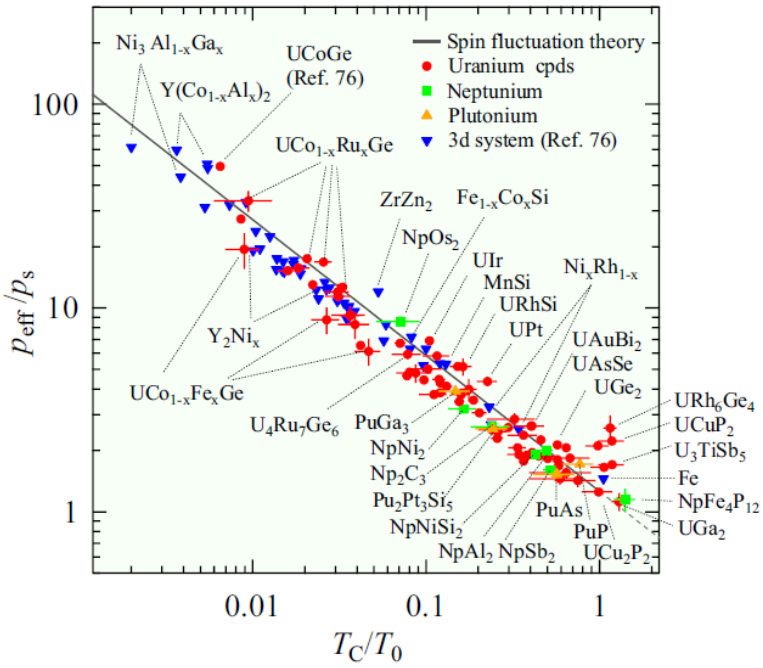

Figure 5.1 Generalized Rhodes-Wohlfarth plot. Data points for uranium, neptunium, and plutonium compounds are plotted as closed circles, squares, and triangles, respectively.

We have analyzed the magnetic data of 69 uranium, 7 neptunium, and 4 plutonium FMs[212] with Takahashi's spin fluctuation theory (Figure 5.1). We have determined the basic and the spin fluctuation parameters of the FMs and discussed the applicability of spin fluctuation theory to the actinide 5*f* electrons system[213, 214]. The ratio of the effective magnetic moment and the spontaneous one, p_{eff}/p_s, follows the generalized Rhodes-Wohlfarth relation, $p_{eff}/p_s \propto (T_C/T_0)^{-3/2}$, predicted by Takahashi's spin fluctuation theory in the actinide ferromagnets for T_C/T_0 <1.0, similarly to itinerant ferromagnets in the 3*d* transition metals and their intermetallics. This result suggests that the itinerant nature of the 5*f* electrons in the actinide FMs and that the magnetic properties of the FMs can be understood in the framework of the spin fluctuation theory. Meanwhile, data points between T_C/T_0 and p_{eff}/p_s deviate from the theoretical relation in several ferromagnets with T_C/T_0 ~1.0, which may be due to the effect of the CEF on the 5*f* electrons. The value

of the spontaneous magnetic moment p_s increases linearly as a function of T_C/T_0 in the uranium and neptunium FMs below (T_C/T_0) kink = 0.32±0.02 where a kink structure appears in the relation between the two quantities. p_s increases more weakly above (T_C/T_0) kink. A possible interpretation with the T_C/T_0-dependence of p_s is given in terms of the Kondo effect.

6 Single crystal growth

Synthesis of the new so far unexplored materials is the key essence for the discovery of new exotic magnetic and electronic states in the field of fundamental physics. Within this scope, I have concentrated to improve the single crystal growth instrumentation in the home institution DCMP within the program of MGML infrastructure. I have contributed to updates of already installed instrumentation (Czochralski method or new monoarc furnace), and I would like to highlight installation of new instruments; SSE, floating zone method implemented in optical furnaces-halogen and laser and multipurpose induction furnace primarily used for Bridgman method in closed Mo-capsules and synthesis of polycrystalline precursors in the form of rods. Nowadays, we invest a lot of effort to implement the chemical vapor transport method (CVT) to grow variants of inorganic salts based on halides and chalcogenides. These activities have resulted in series of cooperations where I contributed by single crystal growth of high-quality single crystals of various classes of materials.

6.1 $UIrSi_3$ [P12]

The RTX_3 compounds with Ce are of high research interest because they exhibit diverse interesting phenomena like superconductivity with a high critical field, pressure-induced SC near a QCP, coexistence of AFM and SC, vibron states, etc.[215-218]. The magnetic ordering in these materials is usually AFM with complex propagation vectors which indicate competing FM and AFM exchange interactions[219-222]. Only two uranium compounds adopting the tetragonal $BaNiSn_3$-type structure were known, namely, $UIrSi_3$ and $UNiGa_3$. Both have been studied in the form of polycrystals only and reported to order antiferromagnetically below 42 K ($UIrSi_3$)[223] and 39 K ($UNiGa_3$)[224], respectively.

We have prepared the first high-quality single crystals of $UIrSi_3$ single crystal by floating zone method[202, 225] to reveal the magnetic and magnetic anisotropy features. The results confirm that $UIrSi_3$ is AFM below the Néel temperature T_N = 41.7 K with a strongly anisotropic response to an external magnetic field. In the magnetic field along the *c* axis, it undergoes a MT at a critical field H_c ($\mu_0 H_c$ = 7.3T at 2 K) into a PPM a magnetic moment of ~0.66 μ_B/f.u. The observed H_c value is much lower than expected for a simple AFM consisting of magnetic moments of the order of 1 μ_B with T_N > 40K. No MT shows up in the *a*-axis field up to 14 T. At low temperatures, MT is FOMPT and shows an asymmetric hysteresis. H_c decreases with increasing temperature while the hysteresis shrinks with increasing temperature and eventually vanishes at 28 K. The character of MT dramatically changes at this temperature from FOMPT to SOMPT which is observed for 28 K > T > T_N) as manifested by the change of character of magnetization and specific-heat anomalies.

We have also performed a detailed study of the electrical resistance, Hall resistance, and thermoelectric power of $UIrSi_3$ at various temperatures and magnetic fields with a special emphasis on phenomena associated with magnetic phase transitions between the antiferromagnetic and paramagnetic states. The obtained results demonstrate that the

electrical and thermal transport properties can provide valuable information on the character of magnetic phase transformations in AFMs.

6.2 $UNi_4{}^{11}B$ [P13]

In the context of frustrated metallic *f* -electron magnets,UNi_4B has been considered as an early hexagonal example[226-228]. Mentink *et al.* reported the system to crystallize in the hexagonal $CeCo_4B$ structure (space group *P6/mmm*) with lattice parameters a = 4.953 and c = 6.964 Å[226]. Here, the uranium ions form a triangular lattice in the hexagonal plane, which might enable magnetic frustration. Thermodynamic studies and neutron scattering[226-228] revealed a magnetic transition at T_N = 20 K. A Curie-Weiss temperature $\Theta_{CW} \sim -65$ K, significantly larger than the ordering temperature T_N, indicates the strong antiferromagnetic interaction predominant in the system and has been taken to be indicative of magnetic frustration[226]. Based on these data, it was argued that the magnetic moments undergo a highly unusual form of partial antiferromagnetic ordering. Only two out of three magnetic moments should participate in long-range magnetic order, resulting in the formation of a vortex-like magnetic structure.

Pulsed-field magnetization data reveal large anisotropy between the measurement parallel and perpendicular to the hexagonal plane (*ab* plane)[227, 228]. The measurements for $B||a$ and $B||b$ show multiple steps in the magnetization. The results were interpreted to the effect that the small magnetization steps are triggered by a slight reorientation of the above-described magnetic structure and that a jump in the magnetization at higher fields is due to an alignment of the magnetic moments along the external magnetic field[227, 228]. More recently, the magnetic structure of UNi_4B was discussed in the context of toroidal order[229].

I have prepared isotopic high-quality $UNi4^{11}B$ single crystal by the floating zone method for the neutron diffraction experiments in ILL Grenoble[230]. The neutron diffraction study has shown that UNi_4B is a rare example of an Ising-like frustrated metallic *f* -electron magnet with a partially ordered magnetic ground state. We have thoroughly characterized the crystal structure of UNi_4B, which turns out to be of lower symmetry than previously reported. We have verified an unusual type of magnetic order, i.e., a vortex-type spin structure of magnetic moments μ_{ord} = 0.99(1)μB/(U atom) on two-thirds of the U sites. The vortex structure carries in it the possibility of toroidal order existing in UNi_4B. In addition, the refinement of the magnetic structure suggests that the magnetic moments are slightly canted compared to the perfect vortex structure.

6.3 Tricriticality in the H-T phase diagram of URhGe [P14]

URhGe is well-known FM SC with intriguing metamagnetic behavior of magnetization along the *b*-axis, which results in the vanishing of FM at magnetic field H_R = 12.4 T. Famous reentrant SC dome appears near H_R due to enhancement of ferromagnetic fluctuations. We have investigated the quantum phase transition of an Ising FM URhGe utilizing high-precision angle-resolved dc magnetization measurements in magnetic fields applied near the *b* axis. I have contributed to work by preparation of suitable single-crystal samples. A first-order spin reorientation transition has been observed at low temperatures, accompanied by a small hysteresis at H_R. The temperature and angular variations of the transition observed in the magnetization as well as in the magnetic torque allow us to construct the three-dimensional T-H_c-H_b phase diagram. The tricritical point T_{TCP} is estimated to be located above 4 K in the H_c = 0 plane. On cooling below T_{TCP}, a wing structure develops by increasing H_c. We have succeeded in directly determining the detailed profiles of the wing structure. The quantum wing critical points exist at H_c = ±1.1 T and H_b = 13.5 T. Three second-order transition lines meet at T_{TCP}

tangentially, so that a precise tuning of H along the b axis within 0.8◦ is needed to correctly determine the position of the TCP. The reentrant superconductivity in this system is not due to a quantum TCP[114], but is rather related to the unusually weak nature of the first-order transition represented by the smallness of the hysteresis and broadness of the transition.

6.4 Ti-alloys [P15-18]

At room temperature and standard pressure, pure titanium crystallizes in a hexagonal close-packed (hcp) structure, which is known as the α phase. This phase is stable up to 883°C. Above this temperature, the structure transforms to a body-centered cubic (bcc) β phase. The stability ranges of α and β phases can be altered and two-phase regions or even new phases can be introduced by adding alloying elements.

Titanium alloys are attractive materials for aerospace, automotive, and biomedical applications due to their outstanding mechanical properties such as high strength in combination with low density. Particularly metastable β-Ti alloys remain of significant interest because of their excellent corrosion resistance, toughness, and good hardenability through ageing treatment[231]. Metastable β-Ti alloys have enough β stabilizer content to retain the high-temperature β phase in a metastable state upon quenching[232]. Moreover, the metastable ω phase with hexagonal structure is formed in metastable β-Ti alloys with a certain content of alloying elements. The ω phase is observed as uniformly dispersed submicron particles which are coherent with the β-Ti matrix. The ω phase is formed during quenching by a diffusionless displacive transformation, which was first described in detail by de Fontaine et al.[233]. The particles of the ω phase further evolve and grow during ageing. This process is accompanied by the rejection of β stabilizing elements from the ω phase; thus this reaction is diffusion controlled. The ω phase particles have an important influence on the mechanical properties of the Ti alloys. Typically, they increase specific strength and hardness but they can also embrittle the material[234]. Furthermore, the ω particles play a significant role in the $\beta \rightarrow \alpha$ phase transformations during ageing at higher temperatures, acting as nucleation sites for the α phase. Consequently, the resulting distribution, size, and volume fraction of the α phase are determined by the preceding ω phase morphology.

Despite a few decades of intensive research on the characteristics of ω phase particles, there is still doubt about the actual causes of ω phase formation. Since the mechanical properties of metastable β-Ti alloys depend strongly on the type and morphology of the particles of secondary phases (i.e. α and ω), the understanding of ongoing phase transformations, ageing kinetics, and their influence on the resulting microstructure is of primary importance. Experimental methods which study these aspects in microscopic scale details require single-crystalline material with known orientation. In particular, the topotaxial relation of the ω and β phases (i.e., the mutual orientation of their lattices) can be studied by x-ray reciprocal space-mapping only in single crystals. For this class of studies by the growth of single crystals of the metastable β-Ti alloys. The floating zone method proved to be a suitable method for the single crystal growth of this type of material. We have determined the crystal structure and quality of the grown crystals by Laue diffraction and EBSD analysis. These experimental techniques confirmed the high quality of the obtained single crystals which were used for series of further advanced experiments[235-238] for research of the ω phase formation.

7 Conclusions

Within the 10 years of the research program, I have collected, in collaboration with my colleagues and students, a large series of experimental results primarily on magnetic features of uranium compounds. We have focused on the effect of external parameters to understand the sensitive interplay of magnetic interactions and electron correlations responsible for the exotic phenomena which were discovered in this class of materials. We have performed series of experiments, in which the chemical substitution, high pressure, and magnetic field were applied primarily on systems based on uranium FM SCs, uranium metamagnets, and other recently studied systems to report their *x*-*T*, *p*-*T*, and *H*-*T* phase diagrams.

We have revealed very complex magnetic behavior in the orthorhombic TiNiSi-type compounds. The external variables are able both to stabilize and to destabilize the magnetic state. Although UCoGe, URhGe, and UIrGe are both isostructural and isoelectronic compounds, their pressure response is unique for each one, supporting the scenario of a strong hybridization of the 5*f* states with the electronic states of surrounding *d*-metals of the various bandwidth. The effect of substitution was found to be a very effective tool to distinguish the differences between the magnetism of parent compounds by the gradual transformation of one magnetic state into another, located on the opposite side of the *T*-*x* phase diagram. Particularly the results of the substitution works, hardly understandable on the level of simple one-electron theories, unravel the complexity and fine balance of magnetic exchange interactions in uranium compounds. The representative case is the response of the hexagonal ZrNiAl-structure type compounds, where the area of stable FM phase of appreciable T_C (exceeding 60 K) develops between two paramagnetic areas in the $UCo_{1-x}Ru_xAl$ system. We have shown that the critical regions where FM vanishes are of different nature on both sides (the UCoAl and URuAl sides).

The conclusions about the magnetism based on standard magnetic and thermodynamic studies were supported by microscopic polarized neutron diffraction studies. We have detected clear signs of the hybridization between the uranium 5*f* and transition-metal *d*-states and described the development of the 5*f* electron itineracy related to the stability of the bulk ferromagnetism in the $UCo_{1-x}Ru_xGe$ and $UCo_{1-x}Ru_xAl$ systems.

The constructed *H*-*T* phase diagrams brought key information about the uranium systems studied. The conventional and advanced high-field experiments highlight the importance of the order and character of the magnetic transitions and crossovers. We have revealed that the magnetic correlations often manifest at temperatures significantly exceeding magnetic ordering temperatures in the uranium systems. Our results clearly show that these so-called correlated paramagnetic regions have a strong impact on the character of low-temperature crossovers, ordinary phase transition, presence of tricriticality, as well as on field-induced metamagnetic phenomena, which are tightly connected with unique superconducting features in FM superconductors.

All the works listed in this thesis also highlighted the necessity of high-quality single crystals and their use in experimental condensed matter research, particularly in the case of highly anisotropic systems. We have succeeded in the preparation of all planed materials to reach the targets of the research program. Within these research activities, the development of the technological laboratories in the Department of Condensed Matter Physics in the section of single crystal growth is the important associated output, to which the author contributed significantly. Examples are installation of a floating zone furnace with laser heating, construction of multifunctional induction furnace for Bridgman

method, and casting of the new materials. The present interest by the author in vdW magnetic materials was projected to implementation of the chemical vapor transport method to the portfolio of the method. All implemented methods are indispensable for progress in the majority of the running project and student research programs at the home department as well as for all users of MGML research infrastructure.

8 Bibliography

[1] B. J. a. H. L. Skriver, *Electronic structure of the actinide metals*, Journal of Magnetism and Magnetic Materials, 1982).

[2] J. L. Sarrao, et al., Nature **420**, 297 (2002).

[3] N. J. Curro, T. Caldwell, E. D. Bauer, L. A. Morales, M. J. Graf, Y. Bang, A. V. Balatsky, J. D. Thompson, and J. L. Sarrao, Nature **434**, 622 (2005).

[4] E. D. Bauer, et al., Journal of Physics-Condensed Matter **24**, 052206 (2012).

[5] E. C. Stoner, Proc. R. Soc. Lond. A **165**, 372 (1938).

[6] J. Pospisil, et al., Physical Review B **102**, 024442 (2020).

[7] H.H.Hill, *Plutonium 1970 and Other Actinides* (ed. W. N.Miner, (American Institute of Mining, Metalurgical, and Petroleum Engeneers, New York), p. 2, 1970).

[8] W. Knafo, Habilitation a Diriger Les Recherches (2021).

[9] V. Sechovsky and L. Havela, in *Handbook of Magnetic Materials*, edited by K. H. J. Buschow (Elsevier, 1998), Vol. Volume 11, p. 1.

[10] D. Belitz, T. R. Kirkpatrick, and T. Vojta, Physical Review Letters **82**, 4707 (1999).

[11] M. Brando, D. Belitz, F. M. Grosche, and T. R. Kirkpatrick, Rev. Mod. Phys. **88**, 025006 (2016).

[12] T. R. Kirkpatrick and D. Belitz, Physical Review B **85**, 134451 (2012).

[13] M. Vojta, Reports on Progress in Physics **66**, 2069 (2003).

[14] H. Löhneysen, Journal of Magnetism and Magnetic Materials **200**, 532 (1999).

[15] S. Sakarya, Magnetic Properties of Uranium Based Ferromagnetic Superconductors, Technische Universiteit Delft, PhD.thesis, 2007.

[16] C. M. Varma, Z. Nussinov, and W. van Saarloos, Physics Reports **361**, 267 (2002).

[17] G. R. Stewart, Reviews of Modern Physics **73**, 797 (2001).

[18] D. Aoki, W. Knafo, and I. Sheikin, C. R. Phys. **14**, 53 (2013).

[19] K. Bakker, A. Devisser, L. T. Tai, A. A. Menovsky, and J. J. M. Franse, Solid State Communications **86**, 497 (1993).

[20] C. Geibel, et al., Physica C **185**, 2651 (1991).

[21] H. R. Ott, H. Rudigier, T. M. Rice, K. Ueda, Z. Fisk, and J. L. Smith, Physical Review Letters **52**, 1915 (1984).

[22] R. A. Fisher, S. Kim, B. F. Woodfield, N. E. Phillips, L. Taillefer, K. Hasselbach, J. Flouquet, A. L. Giorgi, and J. L. Smith, Physical Review Letters **62**, 1411 (1989).

[23] G. Aeppli, D. Bishop, C. Broholm, E. Bucher, K. Siemensmeyer, M. Steiner, and N. Stusser, Physical Review Letters **63**, 676 (1989).

[24] A. De Visser, A. Menovsky, and J. J. M. Franse, Physica B+C **147**, 81 (1987).

[25] J. W. Chen, S. E. Lambert, M. B. Maple, Z. Fisk, J. L. Smith, G. R. Stewart, and J. O. Willis, Physical Review B **30**, 1583 (1984).

[26] J. A. Mydosh and P. M. Oppeneer, Reviews of Modern Physics **83**, 1301 (2011).

[27] T. T. M. Palstra, A. A. Menovsky, and J. A. Mydosh, Phys. Rev. B **33**, 6527 (1986).
[28] M. B. Maple, J. W. Chen, Y. Dalichaouch, T. Kohara, C. Rossel, M. S. Torikachvili, M. W. McElfresh, and J. D. Thompson, Physical Review Letters **56**, 185 (1986).
[29] T. T. M. Palstra, A. A. Menovsky, J. Vandenberg, A. J. Dirkmaat, P. H. Kes, G. J. Nieuwenhuys, and J. A. Mydosh, Physical Review Letters **55**, 2727 (1985).
[30] S. S. Saxena, et al., Nature **406**, 587 (2000).
[31] D. Aoki, A. Huxley, E. Ressouche, D. Braithwaite, J. Flouquet, J. P. Brison, E. Lhotel, and C. Paulsen, Nature **413**, 613 (2001).
[32] N. T. Huy, et al., Physical Review Letters **99**, 067006 (2007).
[33] D. Aoki, et al., Journal of the Physical Society of Japan **88**, 043702 (2019).
[34] S. Ran, et al., Science **365**, 684 (2019).
[35] W. Knafo, M. Valiska, D. Braithwaite, G. Lapertot, G. Knebel, A. Pourret, J. P. Brison, J. Flouquet, and D. Aoki, Journal of the Physical Society of Japan **88**, 063705 (2019).
[36] A. Miyake, et al., Journal of the Physical Society of Japan **88**, 063706 (2019).
[37] W. Knafo, R. Settai, D. Braithwaite, S. Kurahashi, D. Aoki, and J. Flouquet, Physical Review B **95**, 014411 (2017).
[38] D. Aoki, et al., Journal of the Physical Society of Japan **89**, 053705 (2020).
[39] W. Knafo, M. Nardone, M. Valiska, A. Zitouni, G. Lapertot, D. Aoki, G. Knebel, and D. Braithwaite, Communications Physics **4**, 40 (2021).
[40] D. Aoki and J. Flouquet, Journal of the Physical Society of Japan **81**, 011003 (2012).
[41] J. Pospíšil, K. Prokeš, M. Reehuis, M. Tovar, J. P. Vejpravová, J. Prokleška, and V. Sechovský, Journal of the Physical Society of Japan **80**, 084709 (2011).
[42] N. T. Huy, Y. K. Huang, and A. de Visser, Journal of Magnetism and Magnetic Materials **321**, 2691 (2009).
[43] F. Canepa, P. Manfrinetti, M. Pani, and A. Palenzona, Journal of Alloys and Compounds **234**, 225 (1996).
[44] Y. Tokunaga, A. Nakamura, D. Aoki, Y. Shimizu, Y. Homma, F. Honda, H. Sakai, T. Hattori, and S. Kambe, Physical Review B **98**, 014425 (2018).
[45] A. Miyake, L. M. Sandratskii, A. Nakamura, F. Honda, Y. Shimizu, D. X. Li, Y. Homma, M. Tokunaga, and D. Aoki, Physical Review B **98**, 174436 (2018).
[46] D. Mannix, S. Coad, G. H. Lander, J. Rebizant, P. J. Brown, J. A. Paixao, S. Langridge, S. Kawamata, and Y. Yamaguchi, Physical Review B **62**, 3801 (2000).
[47] J. Pospíšil, J. P. Vejpravová, M. Diviš, and V. Sechovský, Journal of Applied Physics **105**, 07E114 (2009).
[48] R. Tro† and V. H. Tran, Journal of Magnetism and Magnetic Materials **73**, 389 (1988).
[49] V. H. Tran, R. Tro†, and D. urski, Journal of Magnetism and Magnetic Materials **87**, 291 (1990).
[50] L. Havela, A. Kolomiets, V. Sechovsky, M. Divis, M. Richter, and A. V. Andreev, Journal of Magnetism and Magnetic Materials **177-181**, 47 (1998).
[51] N. T. Huy, A. Gasparini, J. C. P. Klaasse, A. de Visser, S. Sakarya, and N. H. van Dijk, Physical Review B **75**, 212405 (2007).
[52] N. T. Huy and A. de Visser, Solid State Communications **149**, 703 (2009).
[53] T. R. Kirkpatrick and D. Belitz, Physical Review Letters **115**, 020402 (2015).
[54] J. A. Hertz, Physical Review B **14**, 1165 (1976).
[55] A. J. Millis, Physical Review B **48**, 7183 (1993).

[56] K. Huang, J. J. Hamlin, R. E. Baumbach, M. Janoschek, N. Kanchanavatee, D. A. Zocco, F. Ronning, and M. B. Maple, Physical Review B **87**, 054513 (2013).
[57] M. B. S. Neto, A. H. C. Neto, S. J. Kim, and G. R. Stewart, J. Phys.: Condens. Matter **25**, 025601 (2013).
[58] A. Gasparini, Y. K. Huang, J. Hartbaum, H. von Löhneysen, and A. de Visser, Physical Review B **82**, 052502 (2010).
[59] K. Prokes, A. de Visser, Y. K. Huang, B. Fak, and E. Ressouche, Physical Review B **81**, 180407R (2010).
[60] T. V. Bay, A. M. Nikitin, T. Naka, A. McCollam, Y. K. Huang, and A. de Visser, Physical Review B **89**, 214512 (2014).
[61] K. Prokes and A. Gukasov, Physical Review B **79**, 024406 (2009).
[62] P. Javorsky, V. Sechovsky, J. Schweizer, F. Bourdarot, E. Lelievre-Berna, A. V. Andreev, and Y. Shiokawa, Physical Review B **63**, 064423 (2001).
[63] Y. Takeda, Y. Saitoh, T. Okane, H. Yamagami, T. D. Matsuda, E. Yamamoto, Y. Haga, Y. Onuki, and Z. Fisk, Physical Review B **88**, 075108 (2013).
[64] J. A. Paixão, G. H. Lander, P. J. Brown, H. Nakotte, F. R. de Boer, and E. Brück, Journal of Physics-Condensed Matter **4**, 829 (1992).
[65] J. A. Paixão, G. H. Lander, A. Delapalme, H. Nakotte, F. R. de Boer, and E. Brück, Europhysics Letters **24**, 607 (1993).
[66] *Maximum Entropy and Bayesian Methods* (Kluwer, Dordrecht, 1989).
[67] S. F. Gull and J. Skilling, *MEMSYS III Quantified Maximum Entropy Subroutine Library* (Meldreth, UK, 1989).
[68] R. J. Papoular and B. Gillon, Europhysics Letters **13**, 429 (1990).
[69] M. Taupin, L.-P. Sanchez, J. P. Brison, D. Aoki, G. Lapertot, F. Wilhelm, and A. Rogalev, Physical Review B **92**, 035124 (2015).
[70] M. Taupin, L. Howald, D. Aoki, J. Flouquet, and J. P. Brison, Physical Review B **89**, 041108(R) (2014).
[71] J. Taylor, J. Duffy, M. Butchers, C. Stock, and E. Bauer, Bulletin of the American Physical Society **56**, Z25.9 (2011).
[72] M. Vališka, et al., Journal of the Physical Society of Japan **84**, 084707 (2015).
[73] K. Kaneko, N. Metoki, N. Bernhoeft, G. H. Lander, Y. Ishii, S. Ikeda, Y. Tokiwa, Y. Haga, and Y. Onuki, Physical Review B **68**, 214419 (2003).
[74] O. Eriksson, M. S. S. Brooks, and B. Johansson, Physical Review B **41**, 9087 (1990).
[75] M. Wulff, G. H. Lander, B. Lebech, and A. Delapalme, Physical Review B **39**, 4719 (1989).
[76] K. Prokes, T. Wand, A. V. Andreev, M. Meissner, F. Honda, and V. Sechovsky, Journal of Alloys and Compounds **460**, 47 (2008).
[77] P. Wisniewski, A. Gukasov, Z. Henkie, and A. Wojakowski, Journal of Physics-Condensed Matter **11**, 6311 (1999).
[78] W. Knafo, et al., Physical Review B **86**, 184416 (2012).
[79] F. Levy, I. Sheikin, B. Grenier, and A. D. Huxley, Science **309**, 1343 (2005).
[80] A. Miyake, D. Aoki, and J. Flouquet, Journal of the Physical Society of Japan **78**, 063703 (2009).
[81] A. Miyake, D. Aoki, and J. Flouquet, Journal of the Physical Society of Japan **77**, 094709 (2008).
[82] D. Aoki, G. Knebel, and J. Flouquet, Journal of the Physical Society of Japan **83**, 094719 (2014).
[83] A. Gourgout, A. Pourret, G. Knebel, D. Aoki, G. Seyfarth, and J. Flouquet, Physical Review Letters **117**, 046401 (2016).

[84] S. Nakamura, T. Sakakibara, Y. Shimizu, S. Kittaka, Y. Kono, Y. Haga, J. Pospíšil, and E. Yamamoto, Physical Review B **96**, 094411 (2017).
[85] J. Pospíšil, et al., Physica B: Condensed Matter **536**, 532 (2018).
[86] D. Aoki, T. D. Matsuda, V. Taufour, E. Hassinger, G. Knebel, and J. Flouquet, Journal of the Physical Society of Japan **78**, 113709 (2009).
[87] B. L. Wu, G. Bastien, M. Taupin, C. Paulsen, L. Howald, D. Aoki, and J. P. Brison, Nature Communications **8**, 14480 (2017).
[88] F. Hardy, D. Aoki, C. Meingast, P. Schweiss, P. Burger, H. Von Löhneysen, and J. Flouquet, Physical Review B **83**, 195107 (2011).
[89] D. Braithwaite, D. Aoki, J. P. Brison, J. Flouquet, G. Knebel, A. Nakamura, and A. Pourret, Physical Review Letters **120**, 037001 (2018).
[90] G. Bastien, A. Gourgout, D. Aoki, A. Pourret, I. Sheikin, G. Seyfarth, J. Flouquet, and G. Knebel, Physical Review Letters **117**, 206401 (2016).
[91] G. Bastien, D. Braithwaite, D. Aoki, G. Knebel, and J. Flouquet, Physical Review B **94**, 125110 (2016).
[92] W. Knafo, T. D. Matsuda, F. Hardy, D. Aoki, and J. Flouquet, Physical Review B **100**, 094421 (2019).
[93] J. Pospíšil, et al., Physical Review B **98**, 014430 (2018).
[94] J. Pospíšil, et al., Physical Review B **95**, 155138 (2017).
[95] N. Tateiwa, S. Ikeda, Y. Haga, T. D. Matsuda, E. Yamamoto, K. Sugiyama, M. Hagiwara, K. Kindo, and Y. Onuki, J. Phys. Soc. Jpn. **80**, 014706 (2011).
[96] Y. Hirose, T. Takeuchi, F. Honda, S. Yoshiuchi, M. Hagiwara, E. Yamamoto, Y. Haga, R. Settai, and Y. Onuki, J. Phys. Soc. Jpn. **84**, 074704 (2015).
[97] E. Slooten, T. Naka, A. Gasparini, Y. K. Huang, and A. de Visser, Physical Review Letters **103**, 097003 (2009).
[98] D. Aoki, et al., J.Phys.Soc.Jpn. **80**, SA008 (2011).
[99] M. Vališka, J. Pospíšil, M. Diviš, J. Prokleška, V. Sechovský, and M. M. Abd-Elmeguid, Physical Review B **92**, 045114 (2015).
[100] A. P. Ramirez, B. Batlogg, and E. Bucher, Journal of Applied Physics **61**, 3189 (1987).
[101] S. Yoshii, A. V. Andreev, E. Brück, J. C. P. Klaasse, K. Prokeš, F. R. de Boer, M. Hagiwara, K. Kindo, and V. Sechovský, Journal of Physics: Conference Series **51**, 151 (2006).
[102] Y. Uwatoko, S. Todo, K. Ueda, A. Uchida, M. Kosaka, N. Mori, and T. Matsumoto, Journal of Physics-Condensed Matter **14**, 11291 (2002).
[103] N. Mori, H. Takahashi, and N. Takeshita, High Pressure Res. **24**, 225 (2004).
[104] J. R. Jeffries, R. L. Stillwell, S. T. Weir, Y. K. Vohra, and N. P. Butch, Physical Review B **93**, 184406 (2016).
[105] E. Hassinger, D. Aoki, G. Knebel, and J. Flouquet, Journal of the Physical Society of Japan **77**, 073703 (2008).
[106] K. Prokeš, V. Sechovský, F. R. de Boer, and A. V. Andreev, Journal of Physics-Condensed Matter **20**, 104221 (2008).
[107] K. Prokes, et al., Physica B-Condensed Matter **334**, 272 (2003).
[108] Y. Tokunaga, et al., Physical Review Letters **114**, 216401 (2015).
[109] Y. Shimizu, D. Braithwaite, B. Salce, T. Combier, D. Aoki, E. N. Hering, S. M. Ramos, and J. Flouquet, Physical Review B **91**, 125115 (2015).
[110] A. M. Adamska, L. Havela, Y. Skourski, and A. V. Andreev, Journal of Alloys and Compounds **515**, 171 (2012).
[111] B. Chevalier, B. Lloret, P. Gravereau, B. Buffat, and J. Etourneau, Journal of Magnetism and Magnetic Materials **75**, 13 (1988).

[112] F. R. Deboer, et al., Journal of Applied Physics **69**, 4702 (1991).
[113] F. Hardy, A. Huxley, J. Flouquet, B. Salce, G. Knebel, D. Braithwaite, D. Aoki, M. Uhlarz, and C. Pfleiderer, Physica B-Condensed Matter **359**, 1111 (2005).
[114] F. Levy, I. Sheikin, and A. Huxley, Nature Physics **3**, 460 (2007).
[115] D. Aoki and J. Flouquet, Journal of the Physical Society of Japan **83**, 061011 (2014).
[116] E. A. Yelland, J. M. Barraclough, W. Wang, K. V. Kamenev, and A. D. Huxley, Nature Physics **7**, 890 (2011).
[117] A. V. Andreev, Y. Skourski, S. Yasin, S. Zherlitsyn, and J. Wosnitza, Journal of Magnetism and Magnetic Materials **324**, 3413 (2012).
[118] V. Sechovský, J. Vejpravová, A. Andreev, F. Honda, K. Prokeš, and E. Šantavá, Physica B-Condensed Matter **359**, 1126 (2005).
[119] K. Prokeš, T. Tahara, T. Fujita, H. Goshima, T. Takabatake, M. Mihalik, A. A. Menovsky, S. Fukuda, and J. Sakurai, Physical Review B **60**, 9532 (1999).
[120] D. Gralak and V. H. Tran, Journal of Solid State Chemistry **226**, 50 (2015).
[121] D. Gralak, A. J. Zaleski, and V. H. Tran, Journal of Solid State Chemistry **242**, 175 (2016).
[122] S. Sakarya, et al., Journal of Alloys and Compounds **457**, 51 (2008).
[123] S. Sakarya, N. H. van Dijk, N. T. Huy, and A. de Visser, Physica B-Condensed Matter **378-80**, 970 (2006).
[124] B. Cordero, V. Gomez, A. E. Platero-Prats, M. Reves, J. Echeverria, E. Cremades, F. Barragan, and S. Alvarez, Dalton Trans., 2832 (2008).
[125] K. Prokes, et al., Physica B: Condensed Matter **311**, 220 (2002).
[126] G. H. Lander, M. S. S. Brooks, and B. Johansson, Physical Review B **43**, 13672 (1991).
[127] T. Kawai, et al., J. Phys. Soc. Jpn. **77**, 064717 (2008).
[128] N. T. Huy, D. E. De Nijs, A. Gasparini, J. C. P. Klaasse, A. de Visser, and N. H. van Dijk, Physica B-Condensed Matter **403**, 1260 (2008).
[129] D. Aoki, F. Hardy, A. Miyake, V. Taufour, T. D. Matsuda, and J. Flouquet, Comptes Rendus Physique **12**, 573 (2011).
[130] J. Pospíšil, et al., Journal of the Physical Society of Japan **86**, 044709 (2017).
[131] M. Manago, S. Kitagawa, K. Ishida, K. Deguchi, N. K. Sato, and T. Yamamura, Journal of the Physical Society of Japan **88**, 113704 (2019).
[132] S. Kawamata, K. Ishimoto, Y. Yamaguchi, and T. Komatsubara, Journal of Magnetism and Magnetic Materials **104-107**, 51 (1992).
[133] F. R. de Boer, K. Prokes, H. Nakotte, E. Brück, M. Hilbers, P. Svoboda, V. Sechovsky, L. Havela, and H. Maletta, Physica B **201**, 251 (1994).
[134] V. Sechovsky, et al., Journal of Alloys and Compounds **213-214**, 536 (1994).
[135] X. L. Feng, Q. Zhang, and J. P. Hu, Physical Review B **102**, 140503(R) (2020).
[136] K. Prokeš, V. Sechovský, F. R. de Boer, and A. V. Andreev, Journal of Physics: Condensed Matter **20**, 104221 (2008).
[137] A. Gasparini, Y. K. Huang, N. T. Huy, J. C. P. Klaasse, T. Naka, E. Slooten, and A. de Visser, Journal of Low Temperature Physics **161**, 134 (2010).
[138] D. D. Koelling, B. D. Dunlap, and G. W. Crabtree, Physical Review B **31**, 4966 (1985).
[139] J. M. Fournier, A. Boeuf, P. Frings, M. Bonnet, J. v. Boucherle, A. Delapalme, and A. Menovsky, Journal of the Less Common Metals **121**, 249 (1986).
[140] L. Severin, L. Nordström, M. S. S. Brooks, and B. Johansson, Physical Review B **44**, 9392 (1991).

[141] M. W. Butchers, J. A. Duffy, J. W. Taylor, S. R. Giblin, S. B. Dugdale, C. Stock, P. H. Tobash, E. D. Bauer, and C. Paulsen, Physical Review B **92**, 121107 (2015).
[142] N. T. Huy, D. E. de Nijs, Y. K. Huang, and A. de Visser, Physical Review Letters **100**, 077002 (2008).
[143] K. Prokeš, et al., Physica B: Condensed Matter **311**, 220 (2002).
[144] M. Divis, P. Mohn, K. Schwarz, P. Blaha, and P. Novak, in *1st International Workshop on Electron Correlations and Materials Properties*, Iraklion, Greece, 1998), p. 487.
[145] F. Hardy, A. Huxley, J. Flouquet, B. Salce, G. Knebel, D. Braithwaite, D. Aoki, M. Uhlarz, and C. Pfleiderer, Physica B: Condensed Matter **359-361**, 1111 (2005).
[146] A. Kolomiets, J.-C. Griveau, J. Prchal, A. Andreev, and L. Havela, Physical Review B **91**, 064405 (2015).
[147] B. Chatterjee and J. Kolorenč, Physical Review B **103**, 205146 (2021).
[148] P. Opletal, J. Valenta, P. Proschek, V. Sechovský, and J. Prokleška, Physical Review B **102**, 094409 (2020).
[149] J. Vejpravova-Poltierova, J. Pospisil, J. Prokleska, K. Prokes, A. Stunault, and V. Sechovsky, Physical Review B **82**, 180517R(2010).
[150] M. Míšek, J. Prokleška, P. Opletal, P. Proschek, J. Kaštil, J. Kamarád, and V. Sechovský, AIP Advances **7**, 055712 (2017).
[151] M. Míšek, P. Proschek, P. Opletal, V. Sechovský, J. Kaštil, J. Kamarád, M. Žáček, and J. Prokleška, AIP Advances **8**, 101316 (2018).
[152] V. Sechovsky, L. Havela, H. Nakotte, F. R. de Boer, and E. Bruck, Journal of Alloys and Compounds **207**, 221 (1994).
[153] V. Sechovsky, L. Havela, F. R. de Boer, J. J. M. Franse, P. A. Veenhuizen, J. Sebek, J. Stehno, and A. V. Andreev, Physica B+C **142**, 283 (1986).
[154] V. Sechovsky, L. Havela, P. Nozar, E. Bruck, F. R. de Boer, A. A. Menovsky, K. H. J. Buschow, and A. V. Andreev, Physica B **163**, 103 (1990).
[155] D. Aoki, T. Combier, V. Taufour, T. D. Matsuda, G. Knebel, H. Kotegawa, and J. Flouquet, Journal of the Physical Society of Japan **80**, 094711 (2011).
[156] T. Combier, D. Aoki, G. Knebel, and J. Flouquet, Journal of the Physical Society of Japan **82**, 104705 (2013).
[157] A. Palacio-Morales, A. Pourret, G. Knebel, T. Combier, D. Aoki, H. Harima, and J. Flouquet, Physical Review Letters **110**, 116404 (2013).
[158] K. Karube, T. Hattori, S. Kitagawa, K. Ishida, N. Kimura, and T. Komatsubara, Physical Review B **86**, 024428 (2012).
[159] H. Nohara, et al., Journal of the Physical Society of Japan **80**, 093707 (2011).
[160] O. Eriksson, B. Johansson, and M. S. S. Brooks, Journal of Physics-Condensed Matter **1**, 4005 (1989).
[161] P. Opletal, et al., Npj Quantum Materials **2**, 29 (2017).
[162] N. Kimura, et al., Physical Review B **92**, 035106 (2015).
[163] K. Karube, T. Hattori, K. Ishida, and N. Kimura, Physical Review B **91**, 075131 (2015).
[164] A. V. Andreev, L. Havela, V. Sechovsky, M. I. Bartashevich, J. Sebek, R. V. Dremov, and I. K. Kozlovskaya, Philosophical Magazine B-Physics of Condensed Matter Statistical Mechanics Electronic Optical and Magnetic Properties **75**, 827 (1997).
[165] M. Samsel-Czekala, E. Talik, and R. Troc, Physical Review B **78**, 245120 (2008).
[166] A. V. Andreev, L. Havela, V. Sechovsky, M. I. Bartashevich, T. Goto, and K. Kamishima, Physica B: Condensed Matter **239**, 88 (1997).

[167] M. Valiska, P. Opletal, J. Pospisil, J. Prokleška, and V. Sechovsky, Advances in Natural Sciences: Nanoscience and Nanotechnology **6**, 015017 (2015).
[168] A. V. Andreev, L. Havela, V. Sechovsý, M. I. Bartashevich, T. Goto, and K. Kamishima, Journal of Magnetism and Magnetic Materials **169**, 229 (1997).
[169] A. V. Andreev, I. K. Kozlovskaya, N. V. Mushnikov, T. Goto, V. Sechovsky, Y. Homma, and Y. Shiokawa, Journal of Alloys and Compounds **284**, 77 (1999).
[170] A. V. Andreev, I. K. Kozlovskaya, and V. Sechovsky, Journal of Alloys and Compounds **265**, 38 (1998).
[171] A. V. Andreev, N. V. Mushnikov, T. Goto, V. Sechovský, Y. Homma, and Y. Shiokawa, Physica B: Condensed Matter **329–333**, 499 (2003).
[172] Y. Sang, D. Belitz, and T. R. Kirkpatrick, Physical Review Letters **113**, 207201 (2014).
[173] K. Karube, S. Kitagawa, T. Hattori, K. Ishida, N. Kimura, and T. Komatsubara, Journal of the Physical Society of Japan **83**, 084706 (2014).
[174] T. Vojta, J. Phys. A-Math. Gen. **39**, R143 (2006).
[175] T. Vojta, J. Low Temp. Phys. **161**, 299 (2010).
[176] S. Ubaid-Kassis, T. Vojta, and A. Schröeder, Physical Review Letters **104**, 066402 (2010).
[177] V. Taufour, D. Aoki, G. Knebel, and J. Flouquet, Physical Review Letters **105**, 217201 (2010).
[178] M. Míšek, J. Prokleška, P. Opletal, P. Proschek, J. Kaštil, J. Kamarád, and v. Sechovsky, AIP Advances **7**, 055712 (2016).
[179] J. Pospíšil, et al., Journal of the Physical Society of Japan **85**, 034710 (2016).
[180] N. Tateiwa, Y. Haga, T. D. Matsuda, E. Yamamoto, and Z. Fisk, Physical Review B **89**, 064420 (2014).
[181] P. Javorsky, L. Havela, F. Wastin, P. Boulet, and J. Rebizant, Physical Review B **69**, 054412 (2004).
[182] P. A. Veenhuizen, F. R. de Boer, A. A. Menovsky, V. Sechovsky, and L. Havela, Journal de Physique **49**, 485 (1988).
[183] A. Arrott and J. E. Noakes, Physical Review Letters **19**, 786 (1967).
[184] J. S. Kouvel and M. E. Fisher, Physical Review **136**, 1626 (1964).
[185] F. Mirambet, P. Gravereau, B. Chevalier, L. Trut, and J. Etourneau, Journal of Alloys and Compounds **191**, L1 (1993).
[186] F. R. de Boer, K. Kindo, H. Nakotte, K. Prokes, and V. Sechovsky, Physica B **246**, 129 (1998).
[187] L. Havela, et al., Journal of Applied Physics **76**, 6214 (1994).
[188] V. H. Tran, Z. Zolnierek, A. J. Zaleski, and H. Noël, Solid State Communications **101**, 709 (1997).
[189] R. P. Pinto, M. M. Amado, M. A. Salgueiro, M. E. Braga, J. B. Sousa, B. Chevalier, F. Mirambet, and J. Etourneau, Journal of Magnetism and Magnetic Materials **140**, 1371 (1995).
[190] P. D. du Plessis, A. M. Strydom, and V. H. Tran, Solid State Communications **112**, 391 (1999).
[191] L. Havela, et al., Journal of Magnetism and Magnetic Materials **140**, 1367 (1995).
[192] A. M. Strydom and P. D. du Plessis, Physica B **230**, 62 (1997).
[193] L. M. Sandratskii, Physical Review B **94**, 184414 (2016).
[194] L. M. Sandratskii, Physica B-Condensed Matter **536**, 512 (2018).
[195] D. Kaczorowski and L. D. Gulay, Journal of Alloys and Compounds **419**, 11 (2006).

196 J. Pospíšil, M. Míšek, M. Diviš, M. Dušek, F. R. de Boer, L. Havela, and J. Custers, Journal of Alloys and Compounds **823**, 153485 (2020).
197 K. Prokes, et al., Physical Review B **95**, 174433 (2017).
198 L. C. J. Pereira, J. A. Paixao, P. Estrela, M. Godinho, F. Boudarot, M. Bonnet, J. Rebizant, J. C. Spirlet, and M. Almeida, Journal of Physics-Condensed Matter **8**, 11167 (1996).
199 K. Prokes, et al., Physica B **294**, 288 (2001).
200 A. Purwanto, et al., Physical Review B **50**, 6792 (1994).
201 F. Honda, J. Valenta, J. Prokleska, J. Pospisil, P. Proschek, J. Prchal, and V. Sechovsky, Physical Review B **100**, 014401 (2019).
202 J. Valenta, et al., Physical Review B **97**, 144423 (2018).
203 E. Brück, et al., Journal of Magnetism and Magnetic Materials **104**, 17 (1992).
204 K. Shrestha, D. Antonio, M. Jaime, N. Harrison, D. S. Mast, D. Safarik, T. Durakiewicz, J. C. Griveau, and K. Gofryk, Scientific Reports **7**, 6642 (2017).
205 R. L. Stillwell, I. L. Liu, N. Harrison, M. Jaime, J. R. Jeffries, and N. P. Butch, Physical Review B **95**, 014414 (2017).
206 E. Brück, et al., Physical Review B **49**, 8852 (1994).
207 R. Bruinsma and G. Aeppli, Physical Review B **29**, 2644 (1984).
208 S. Mašková, et al., Physical Review B **99**, 064415 (2019).
209 P. Santini, R. Lemanski, and P. Erdos, Advances in Physics **48**, 537 (1999).
210 P. Santini, S. Carretta, G. Amoretti, R. Caciuffo, N. Magnani, and G. H. Lander, Rev. Mod. Phys. **81**, 807 (2009).
211 K. T. Moore and G. van der Laan, Rev. Mod. Phys. **81**, 235 (2009).
212 N. Tateiwa, J. Pospisil, Y. Haga, H. Sakai, T. D. Matsuda, and E. Yamamoto, Physical Review B **96**, 035125 (2017).
213 Y. Takahashi, Journal of the Physical Society of Japan **55**, 3553 (1986).
214 Y. Takahashi, Journal of Physics-Condensed Matter **13**, 6323 (2001).
215 N. Kimura, K. Ito, K. Saitoh, Y. Umeda, H. Aoki, and T. Terashima, Physical Review Letters **95**, 247004 (2005).
216 M. Klicpera, D. T. Adroja, K. Vlaskova, M. Boehm, H. Mutka, B. Ouladdiaf, T. Guidi, and P. Javorsky, Inorganic Chemistry **56**, 12839 (2017).
217 C. Pfleiderer, Reviews of Modern Physics **81**, 1551 (2009).
218 I. Sugitani, et al., Journal of the Physical Society of Japan **75**, 043703 (2006).
219 N. Aso, M. Takahashi, H. Yoshizawa, H. Iida, N. Kimura, H. Aoki, and Iop, Journal of Physics Conference Series **400**, 022003 (2012).
220 M. Klicpera, P. Javorsky, P. Cermak, A. Schneidewind, B. Ouladdiaf, and M. Divis, Physical Review B **91**, 224419 (2015).
221 M. Smidman, et al., Physical Review B **88**, 134416 (2013).
222 D. Ueta, Y. Ikeda, and H. Yoshizawa, Journal of the Physical Society of Japan **85** (2016).
223 B. Buffat, B. Chevalier, B. Czeska, J. Etourneau, and P. Hagenmuller, Journal of Magnetism and Magnetic Materials **62**, 53 (1986).
224 T. Takabatake, et al., Physica B-Condensed Matter **186-88**, 734 (1993).
225 F. Honda, J. Valenta, J. Prokleška, J. Pospíšil, P. Proschek, J. Prchal, and V. Sechovský, Physical Review B **100**, 014401 (2019).
226 S. A. M. Mentink, A. Drost, G. J. Nieuwenhuys, E. Frikkee, A. A. Menovsky, and J. A. Mydosh, Physical Review Letters **73**, 1031 (1994).
227 S. A. M. Mentink, T. E. Mason, A. Drost, E. Frikkee, B. Becker, A. A. Menovsky, and J. A. Mydosh, Physica B-Condensed Matter **223-24**, 237 (1996).

[228] S. A. M. Mentink, G. J. Nieuwenhuys, H. Nakotte, A. A. Menovsky, A. Drost, E. Frikkee, and J. A. Mydosh, Physical Review B **51**, 11567 (1995).
[229] H. Saito, K. Uenishi, N. Miura, C. Tabata, H. Hidaka, T. Yanagisawa, and H. Amitsuka, Journal of the Physical Society of Japan **87**, 033702 (2018).
[230] J. Willwater, et al., Physical Review B **103**, 184426 (2021).
[231] P. J. Bania, Jom-Journal of the Minerals Metals & Materials Society **46**, 16 (1994).
[232] J. C. W. G. Lütjering, Titanium,Springer-Verlag,Berlin,2007.
[233] D. De Fontaine, N. E. Paton, and J. C. Williams, Acta Metallurgica **19**, 1153 (1971).
[234] T. Sakamoto, K. Nakai, M. Maeda, and S. Kobayashi, 6th Pacific Rim International Conference on Advanced Materials and Processing **561-565**, 2067 (2007).
[235] J. Smilauerova, P. Harcuba, J. Pospisil, Z. Matej, and V. Holy, Acta Materialia **61**, 6635 (2013).
[236] J. Smilauerova, et al., Acta Materialia **81**, 71 (2014).
[237] J. Smilauerova, J. Pospisil, P. Harcuba, V. Holy, and M. Janecek, Journal of Crystal Growth **405**, 92 (2014).
[238] P. Strunz, J. Smilauerova, M. Janecek, J. Strasky, P. Harcuba, J. Pospisil, J. Vesely, P. Lindner, and L. Karge, Philosophical Magazine **98**, 3086 (2018).

9 List of attached publications [P1-18]

[P1] Evolution of ferromagnetic and non-Fermi-liquid states with doping: The case of Ru-doped UCoGe, M. Vališka, J. Pospíšil, M. Diviš, J. Prokleška, V. Sechovský, and M. M. Abd-Elmeguid, Physical Review B - Condensed Matter and Materials Physics **92** (2015) 045114;
DOI: 10.1103/PhysRevB.92.045114

[P2] Gradual localization of 5f states in orthorhombic UTX ferromagnets: Polarized neutron diffraction study of Ru substituted UCoGe,M. Vališka, J. Pospíšil, A. Stunault, Y. Takeda, B. Gillon, Y. Haga, K. Prokeš, M. M. Abd-Elmeguid, G. Nénert, T. Okane, H. Yamagami, L. Chapon, A. Gukasov, A. Cousson, E. Yamamoto, and V. Sechovský, Journal of the Physical Society of Japan **84** (2015) 084707; DOI: 0.7566/JPSJ.84.084707

[P3] Intriguing behavior of $UCo_{1-x}Rh_xGe$ ferromagnets in magnetic field along the b axis, J. Pospisil, Y. Haga, A. Miyake, S. Kambe, Y. Tokunaga, M. Tokunaga, E. Yamamoto, P. Proschek, J. Volny, and V. Sechovsky, Physical Review B **102** (2020) 024442; DOI: 10.1103/PhysRevB.102.024442

[P4] Effect of pressure on magnetism of UIrGe, J. Pospisil, J. Gouchi, Y. Haga, F. Honda, Y. Uwatoko, N. Tateiwa, S. Kambe, S. Nagasaki, Y. Homma, and E. Yamamoto, Journal of the Physical Society of Japan **86** (2017) 044709;
DOI: 10.7566/JPSJ.86.044709

[P5] Magnetic field induced phenomena in UIrGe in fields applied along the b axis, J. Pospíšil, Y. Haga, Y. Kohama, A. Miyake, S. Kambe, N. Tateiwa, M. Vališka, P. Proschek, J. Prokleška, V. Sechovský, M. Tokunaga, K. Kindo, A. Matsuo, and E. Yamamoto, Physical Review B **98** (2018) 014430;
DOI: 10.1103/PhysRevB.98.014430

[P6] Switching of magnetic ground states across the $UIr_{1-x}Rh_xGe$ alloy system, J. Pospíšil, Y. Haga, S. Kambe, Y. Tokunaga, N. Tateiwa, D. Aoki, F. Honda, A. Nakamura, Y. Homma, E. Yamamoto, and T. Yamamura, Physical Review B **95** (2017) 155138; DOI: 10.1103/PhysRevB.95.155138

[P7] Alloying driven transition between ferro- and antiferromagnetism in UTGe compounds: the $UCo_{1-x}Ir_xGe$ case, D. Hovančík, A. Koriki, A. Bendová, P. Doležal, P. Proschek, M. Míšek, M. Reiffers, J. Prokleška, J. Pospíšil, and V. Sechovský, In review proces in Physical Review B

[P8] Properties and collapse of the ferromagnetism in $UCo_{1-x}Ru_xAl$ studied in single crystals, J. Pospíšil, P. Opletal, M. Vališka, Y. Tokunaga, A. Stunault, Y. Haga, N. Tateiwa, B. Gillon, F. Honda, T. Yamamura, V. Nižnanský, E. Yamamoto, and D. Aoki, Journal of the Physical Society of Japan **85** (2016) 034710;
DOI: 10.7566/JPSJ.85.034710

[P9] Critical behavior of magnetization in URhAl: Quasi-two-dimensional Ising system with long-range interactions, N. Tateiwa, J. Pospíšil, Y. Haga, and E. Yamamoto, Physical Review B **97** (2018) 064423;
DOI: 10.1103/PhysRevB.97.064423

[P10] Magnetic phase diagram of the antiferromagnet U_2Rh_2Pb, J. Pospisil, M. Misek, M. Divis, M. Dusek, F. R. de Boer, L. Havela, and J. Custers, Journal of Alloys and Compounds **823** (2020) 153485;
DOI: 10.1016/j.jallcom.2019.153485

[P11] Itinerant ferromagnetism in actinide 5f -electron systems: Phenomenological analysis with spin fluctuation theory, N. Tateiwa, J. Pospíšil, Y. Haga, H. Sakai, T. D. Matsuda, and E. Yamamoto, Physical Review B **96** 035125 (2017) 035125;
DOI: 10.1103/PhysRevB.96.035125

[P12] Magnetotransport as a probe of phase transformations in metallic antiferromagnets: The case of $UIrSi_3$, F. Honda, J. Valenta, J. Prokleska, J. Pospisil, P. Proschek, J. Prchal, and V. Sechovsky, Physical Review B **100** (2019) 014401; DOI: 10.1103/PhysRevB.100.014401

[P13] Crystallographic and magnetic structure of UNi_4B^{11}, J. Willwater, S. Sullow, M. Reehuis, R. Feyerherm, H. Amitsuka, B. Ouladdiaf, E. Suard, M. Klicpera, M. Valiska, J. Pospisil, and V. Sechovsky, Physical Review B **103** 184426 (2021) 184426;
DOI: 10.1103/PhysRevB.103.184426

[P14] Wing structure in the phase diagram of the Ising ferromagnet URhGe close to its tricritical point investigated by angle-resolved magnetization measurements, S. Nakamura, T. Sakakibara, Y. Shimizu, S. Kittaka, Y. Kono, Y. Haga, J. Pospíšil, and E. Yamamoto, Physical Review B **96** (2017) 094411;
DOI: 10.1103/PhysRevB.96.094411

[P15] Growth of ω inclusions in Ti alloys: An X-ray diffraction study, J. Šmilauerová, P. Harcuba, J. Pospíšil, Z. Matěj, and V. Holý, Acta Materialia **61** (2013) 6635;
DOI: 10.1016/j.actamat.2013.07.059

[P16] Single crystal growth of TIMETAL LCB titanium alloy by a floating zone method, J. Šmilauerová, J. Pospíšil, P. Harcuba, V. Holý, and M. Janeček, Journal of Crystal Growth **405** (2014) 92;
DOI: 10.1016/j.jcrysgro.2014.07.050

[P17] Ordered array of ω particles in β-Ti matrix studied by small-angle X-ray scattering, J. Šmilauerová, P. Harcuba, J. Stráský, J. Stráská, M. Janeček, J. Pospíšil, R. Kužel, T. Brunátová, V. Holý, and J. Ilavský, Acta Materialia **81** (2014) 71;
DOI: 10.1016/j.actamat.2014.06.042

[P18] Evaluation of anisotropic small-angle neutron scattering data from metastable β-Ti alloy, P. Strunz, J. Šmilauerová, M. Janeček, J. Stráský, P. Harcuba, J. Pospíšil, J. Veselý, P. Lindner, and L. Karge, Philosophical Magazine **98** (2018) 3086; DOI: 10.1080/14786435.2018.1520403

10 Appendix - Attached publications [P1]-[P18]

(Removed from this version)